New Jersey Institute of Technology

Digital Commons @ NJIT

Spring 5-31-2006

Network activity arising from optimal diameters of neuronal processes

Juliane Gansert
New Jersey Institute of Technology

Follow this and additional works at: https://digitalcommons.njit.edu/theses

Part of the Biostatistics Commons, and the Computer Sciences Commons

Recommended Citation

ABSTRACT

NETWORK ACTIVITY ARISING FROM OPTIMAL DIAMETERS OF NEURONAL PROCESSES

by
Juliane Gansert

Electrical coupling provides an important pathway for signal transmission between neurons. In several regions of the mammalian brain electrical synapses have been detected, and their role in the synchronization of neural networks and the generation of oscillations has been studied theoretically. Recently, it has been found that the amplitude of the postsynaptic potential is maximized for a specific diameter of the postsynaptic fiber.

In this thesis, the impact of the fiber's diameter on the success or failure of the action potential initiation and propagation is studied theoretically. Systems of two coupled neurons, as well as small networks, are investigated. The passive and voltage-dependent properties of the neurons are implemented using compartment modeling. The results of the simulations show that for neurons with non-branching dendrites an action potential is initiated only for a specific, optimal diameter. In contrast, for neurons with branching structures the signal transmission improves monotonically with increasing diameter. By studying a model network with a ring architecture it is demonstrated that network activity crucially depends on the diameter of the coupled fibers.

NETWORK ACTIVITY ARISING FROM OPTIMAL DIAMETERS OF NEURONAL PROCESSES

by
Juliane Gansert

A Thesis
Submitted to the Faculty of
New Jersey Institute of Technology
in Partial Fulfillment of the Requirements for the Degree of
Master of Science in Computational Biology

Department of Computer Science
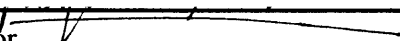
May 2006

Blank Page

**NETWORK ACTIVITY ARISING FROM OPTIMAL DIAMETERS OF
NEURONAL PROCESSES**

Juliane Gansert

Dr. Farzan Nadim, Thesis Advisor   Date
Associate Professor, Dept. of Mathematical Sciences, NJIT
Dept. of Biological Sciences, Rutgers University

Prof. Jason Wang, Committee Member   Date
Professor, Dept. of Computer Science, NJIT

Dr. Marc Ma, Committee Member   Date
Assistant Professor, Dept. of Computer Science, NJIT

BIOGRAPHICAL SKETCH

Author: Juliane Gansert

Degree: Master of Science

Date: May 2006

Undergraduate and Graduate Education:

- Master of Science in Computational Biology,
  New Jersey Institute of Technology, Newark, NJ, 2006

- Bachelor of Science in Computational Life Science,
  University Lübeck, Lübeck, Germany, 2005

Major: Computational Biology

To a special transatlantic relationship.

ACKNOWLEDGMENT

First of all, I would like to thank Dr. Farzan Nadim for his advisement on this thesis and the software he provided for my work. He gave me the chance to jump into the field of Computational Neurobiology, which was completely new to me. Working under his leadership was a great experience, and I gained a lot from my discussions with him.

Also, I would like to thank Prof. Jason Wang for his serving on my thesis committee and for the opportunity to work on research topics under his guidance during my first semester at NJIT.

I want to express my gratitude to Dr. Marc Ma for his support throughout my studies in the program Computational Biology, especially for the discussions regarding my future academic education, and for agreeing to be part of my thesis committee.

Of invaluable importance was Dr. Jorge Golowasch whose patience and support is highly appreciated. His seminal advice was crucial, and I am grateful for the time he took to assist me in honing my models and this thesis.

I am deeply indebted to my family and friends for their constant support and encouragement. Most of all, I would like to thank Chris for his love, patience, and his faith in me.

I am very grateful to the people who helped to improve the writing in this thesis: Mrs. Janet Bodner reminded me of using the grammatical article, my younger brother, Matthias, identified sections where clarification was needed, and my friend and roommate, C. J. Ondek, patiently proofread the entire document. Thank you!

This thesis would not exist without the financial support of the German Fulbright Commission, who covered tuition, fees and maintenance during my two semesters of graduate studies at NJIT.

TABLE OF CONTENTS

TABLE OF CONTENTS
(Continued)

LIST OF FIGURES

LIST OF SYMBOLS

λ	Length constant (cm)
τ	Time constant (s)
C_m	Specific membrane capacitance ($\frac{F}{cm^2}$)
d	Diameter of the cable (cm)
F	Faraday constant ($F = 96,485\frac{C}{mol}$)
I_0	Input current (pA)
R	Thermodynamic gas constant ($R = 8.31\frac{J}{K\,mol}$)
R_i	Specific intracellular resistance (Ωcm)
R_{in}	Input resistance (Ω)
R_∞	Input resistance of a semi-infinite cable (Ω)
R_m	Specific membrane resistance (Ωcm^2)
R_T	Terminating resistance (Ω)
T	Absolute temperature (K)
V	Transmembrane potential relative to V_{rest} (mV)
V_m	Membrane potential (mV)
V_{rest}	Membrane resting potential (mV)

CHAPTER 1

INTRODUCTION

Neurons, the primary units of the nervous system, are capable of responding to internal or external stimuli by generating electrical signals. Neurons form interacting networks, which enable them to spread signals over long distances and perform complex computations. It is now accepted that signals between two neurons are conducted chemically as well as electrically (Hormuzdi et al., 2004; LeBeau et al., 2003; Zoidl and Dermietzel, 2002).

In the human brain electrical synapses are prevalent in several regions, and it has been shown that electrical coupling is crucial for network activity (Sharp, Abbott, and Marder, 1992; LeBeau et al., 2003; Zhang and Poo, 2001; Zoidl and Dermietzel, 2002). Due to its presumed importance in behavior, memory, sensory perception, motor activity, and learning, electrical coupling has been studied experimentally and analytically (Traub et al., 2003; Traub et al., 2001; Zoidl and Dermietzel, 2002; LeBeau et al., 2003; Hormuzdi et al., 2004). It is fundamental to understand how the synaptic and intrinsic properties are interrelated and produce the output that is observed.

The influence of the coupling strength has been examined, and it has been demonstrated that weak electrical coupling can decrease synchronization and result in out-of-phase firing (Sharp, Abbott, and Marder, 1992; Marder, 1998). Fukuda and Kosaka (2003) studied the ultrastructural characteristics of gap junctions in the neocortex, proposed values for the diameters of the connected fibers and the location of the gap junction, and estimated its conductance. However, it is difficult to experimentally examine the consequences of changes in the morphology of the neurons on the signal propagation. In a recent study, Nadim and Golowasch (2006) showed analytically that the signal transmission across the electrical synapse is maximized for an optimal diameter of the postsynaptic fiber.

This thesis demonstrates that in neurons without a branching structure an action potential is initiated only if the dendrite has the specific, optimal diameter. In contrast, an optimal diameter does not exist for neurons with several dendrites branching from

one node. In the case of branching the signal transmission improves monotonically with increasing diameter. Studying ring models of six or 10 neurons, it is shown that the successful propagation of electrical signals requires a specific diameter of the coupled fibers.

This thesis is organized in the following manner. Chapter 2 provides an introduction to the anatomy of a neuron, addresses its electrical properties, and reviews the electrical synapse. The passive characteristics of a neuron are modeled using linear cable theory in Chapter 3. In addition, this chapter presents the concept of compartment modeling and introduces the Hodgkin-Huxley model to represent membranes with voltage-dependent properties. Chapter 4 is devoted to propose the investigated models and to present the obtained results. The concluding chapter of this thesis summarizes the results and provides suggestions for further studies.

CHAPTER 2

BIOLOGICAL BACKGROUND

Neurons are the fundamental units in the nervous system. This chapter is devoted to provide a basic understanding of their characteristics. In Section 2.1 an introduction into the anatomy of a neuron is given, in Section 2.2 the neuron's electrical properties are described, which are integral for its role in signaling. The last section of this chapter addresses the characteristics of electrical synapses, which are the objectives of this thesis.

2.1   The Neuron

Neurons are cells specialized in generating and propagating signals in response to chemical, electrical, or other stimuli such as stretch or pressure. In the human nervous system about 10^{12} neurons can be found, showing extensive morphological and functional diversity.

As schematically illustrated in Figure 2.1, a neuron consists of a roughly spherical cell body called the soma, which extends and branches to its neurites – an axon and one or more dendrites. The soma contains the nucleus, as well as other intracellular organelles, and is the place of protein synthesis. The soma of a typical cortical neuron in a mouse is about 10-50μm in diameter (Dayan and Abbott, 2001). The dendrites form a treelike structure and generally receive input from other neurons or the environment. These input signals are propagated toward the soma. Every nerve cell has only a single axon which can, however, branch extensively to target numerous cells. Axons vary greatly in length. In the cortical cells of the mouse, the total length of the axon fibers of a single neuron is estimated to be 40mm, approximately four times as much as the total length of the dendrites (Dayan and Abbott, 2001). Some human motoneurons can be over a meter in length, and those of large animals can even reach farther. Yet, some neurons have extensive dendritic trees that contain up to 98% of the entire surface area of the neuron (Koch, 1999). The part of the axon that is the closest to the soma is called the axon hillock. Having a huge number of voltage-dependent sodium channels, it is the area of the neuron that is most
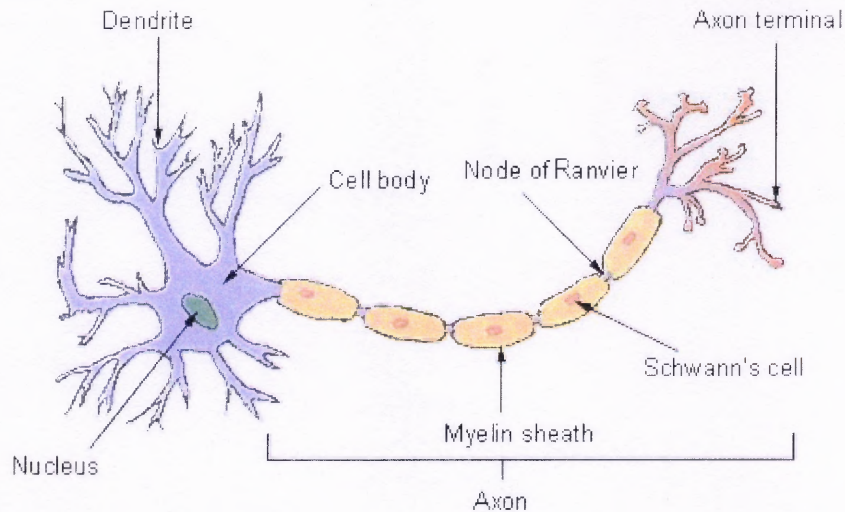
Figure 2.1 Structure of a neuron, by courtesy of Young (no date).

easily depolarized. Here, action potentials are initiated to propagate along the length of the axon to the terminals, where contact to other cells is made. Some axons are covered with a myelin sheath formed by glial cells. By reducing the membrane capacitance and increasing the membrane resistance, the sheath enables the cell to conduct impulses faster. The myelin sheath is interspersed by gaps of less than 1μm in length called the nodes of Ranvier, where a large number of voltage-dependent sodium channels accumulate (Arroyo and Scherer, 2000). Here, the action potential is refreshed by an inward sodium current and flows passively down the myelin-covered sections to the next node. Since the signal "jumps" from node to node, this way of signal transmission is called saltatory conduction. It is much faster and metabolically less consuming than propagation in unmyelinated fibers, where the impulse moves continuously down the axon.

Like every biological membrane, the cell membrane of a neuron consists of a semi-permeable bilayer of phospholipid molecules and proteins. The 3-5nm thick cell membrane isolates the external from the intracellular fluid (cytoplasm). The membrane is essentially impermeable to most charged molecules and therefore acts like a capacitor by separating ionic charges across the surfaces (Koch, 1999). Additionally, the membrane is spanned by ion channels that are more or less specific for sodium (Na^+), potassium (K^+), chloride (Cl^-) and calcium (Ca^{2+}) ions. The ion channels are capable of gating the flow of ions

across the cell membrane by opening and closing specifically in response to voltage changes and to internal or external stimuli such as neurotransmitters. Therefore, ion channels represent a varying resistance of the membrane to ionic flux. For example, if an incoming stimulus depolarizes the membrane to a certain threshold, the conductance of the voltage-gated ion channels quickly changes. The neuron fires an action potential, which is essential for the transmission of electrical impulses over long distances. The ionic basis of the action potential and its generation is described in Section 2.2.

Communication between a presynaptic axon terminal and a dendrite, the soma, or less frequently, the axon of the target cell, occurs at specialized contact zones called synapses. Each neuron in the mammalian brain makes about 1,000 connections to other neurons and receives input from even more (Kandel, Schwartz, and Jessell, 2000). At the synapse, the communicated signal is either inhibitory or excitatory, leading to decreased or increased activity in the postsynaptic cell. Additionally, there are two distinct ways of transmission. A signal is conducted chemically or electrically. Two chemically coupled neurons are separated by a synaptic cleft of about 20-40nm (Hormuzdi et al., 2004). An action potential arriving at the axon terminal triggers the release of neurotransmitters from the presynaptic membrane into the synaptic cleft. At the postsynaptic cell, these molecules bind to specific receptors which in turn change the membrane conductance by either opening or closing the ion channels. In contrast, the intracellular fluid of electrically coupled neurons is connected directly by channel proteins, which allow the flow of ions and other small molecules. Electrical synapses are found more frequently than has been conjectured previously (Hormuzdi et al., 2004). This form of connection is discussed in detail in Section 2.3.

A good part of today's knowledge about the signal transmission in neurons is a result of studying the giant axon of the squid, which proves an ideal experimental preparation due to its size – several centimeters long with a diameter of 0.5 to 1mm.

2.2 Electrical Properties of Nerve Cells

Signaling in the nervous system is based on the potential difference across the cell membrane of a neuron. The membrane potential is the result of the selective permeability of the membrane and an uneven ion distribution inside and outside the cell. In Section 2.2.1 the ionic basis of the resting potential is discussed, and in Section 2.2.2 the generation of the action potential is addressed.

2.2.1 Ionic Distribution and the Membrane Resting Potential

The potential difference between the extracellular fluid and the cytoplasm is an intrinsic property of all cells; however, in non-excitable cells the potential does not change appreciably over time. In contrast, neuronal signaling is based on rapid changes of the membrane potential.

By convention the extracellular fluid is grounded (0mV), and the membrane potential V_m is measured as the difference between the internal and external voltage. At rest, when the cell is in dynamic equilibrium, there is an accumulation of negative charge inside and positive charge outside most cells. The cytoplasm is populated by many negatively charged, large proteins and amino acids which cannot leave the cell because of their size. In most animal cells the following holds true for the concentration of the major ions:

$[K^+]_{in} > [K^+]_{out}$, $[Na^+]_{in} < [Na^+]_{out}$, $[Cl^-]_{in} < [Cl^-]_{out}$, and $[Ca^{2+}]_{in} < [Ca^{2+}]_{out}$. This ionic distribution results in a negative resting potential V_{rest} of about -55mV to -70mV.

At rest, some of the potassium channels are open, allowing K^+ ions to move across the membrane. On the one hand, movement of potassium ions out of the cell is favored, since the external concentration is much lower than the internal concentration. On the other hand, the negative charge inside the cell, which increases as K^+ ions leave the cell, pulls them back in. When both forces on K^+ ions – the concentration gradient and the electrical gradient – are balanced, there is no net flux of potassium ions across the membrane and the equilibrium potential for potassium is reached. For a membrane that can only be crossed by a single ion species i, the equilibrium potential E_i at which the net flux across the

membrane is zero is given by the Nernst equation:

$$E_i = \frac{RT}{z_i F} \ln \frac{[i]_{out}}{[i]_{in}}.$$ (2.1)

$[i]_{out}$ and $[i]_{in}$ are the extra- and intracellular concentrations of the ion i, R is the thermo-dynamic gas constant ($R = 8.31 \frac{J}{K \, mol}$), T is the absolute temperature (K), z_i is the valence of the ion i, and F is the Faraday constant ($F = 96,485 \frac{C}{mol}$). E_K, the equilibrium potential of potassium, lies typically between -70mV and -90mV; E_{Na} =50mV, E_{Ca} =150mV and E_{Cl} =-65mV (Dayan and Abbott, 2001). $V_m - E_i$ is called the electrochemical driving force of the ion i, and is often compared to a battery. Since the direction of current flow changes when the membrane potential V_m passes through E_i, E_i is called the reversal potential. If V_m and E_i are equal, there is no net flux of the ion i across the membrane.

In general, the membrane is permeable to more than a single ion species, and a potential that results in zero net flux does not simply imply that the current for each single ion is balanced. Thus, the Nernst equation cannot be used to calculate the exact value of the membrane potential at equilibrium. As a variation of the Nernst equation, the Goldman-Hodgkin-Katz (GHK) equation approximates V_m by taking into account all ionic currents under the assumption of a constant electric field:

$$V_m = \frac{RT}{F} \ln \frac{P_K[K^+]_{out} + P_{Na}[Na^+]_{out} + P_{Cl}[Cl^-]_{in}}{P_K[K^+]_{in} + P_{Na}[Na^+]_{in} + P_{Cl}[Cl^-]_{out}},$$

where P_i is the permeability of the ion i. A detailed derivation of the GHK equation can be found in Keener and Sneyd (2001). In the resting state the permeability of the membrane to potassium ions dominates the permeability to the other ions. Because of that, the resting potential V_{rest} is close to the potassium equilibrium potential E_K.

However, at rest some sodium channels are open, leading to a slow leak current of sodium into the cell. This leak current is enforced by both the concentration gradient and the electrical gradient. In turn, potassium ions can leave the cell more easily. Since this would eventually eliminate the concentration gradient for potassium, the cell is equipped with passive and active mechanisms in order to maintain the concentration gradients.

The energy-dependent, electrogenic sodium-potassium-pump is the most important ion transporter in neurons. It pumps three Na^+ ions out, in exchange for two K^+ ions in, and is the main reason for the maintenance of the high internal concentration of potassium and the high external concentration of sodium.

Additionally, K^+ ions are attracted into the cell and Cl^- ions are repelled because of the large amount of negatively charged proteins in the cell and the principle of space-charge neutrality. This results in a higher concentration of potassium inside than outside and a high external chloride concentration.

Besides, numerous other passive processes as well as active pumps and transporter molecules in the plasma membrane maintain the ion distribution and the negative resting potential. A detailed description of these transport mechanisms can be found in Nicholls et al. (2001).

2.2.2 The Action Potential

If a neuron is quickly depolarized by a stimulus to a certain threshold, it produces an action potential. Bernstein (1902) hypothesized that an action potential is the result of a breakdown of the membrane potential, leading to a voltage of 0mV. Forty years later Curtis and Cole (1942) and Hodgkin and Huxley (1945) refuted this hypothesis by showing that the inside of the cell becomes positive with respect to the extracellular fluid.

A depolarizing stimulus triggers the voltage-gated sodium channels to open. Na^+ ions enter the cell through the open channels, depolarize the cell further and, by positive feedback, cause even more sodium channels to open. Once the membrane has been depolarized to a certain threshold, voltage-dependent potassium channels open and sodium channels are inactivated. Potassium ions leaving the neuron as a result of their electro-chemical gradient hyperpolarize the cell membrane before ion pumps restore the membrane resting potential.

For a few milliseconds after an action potential, it is impossible to initiate another one due to the inactivation of the sodium channels and the activation of the potassium channels. This is called the absolute refractory period. During the relative refractory period which
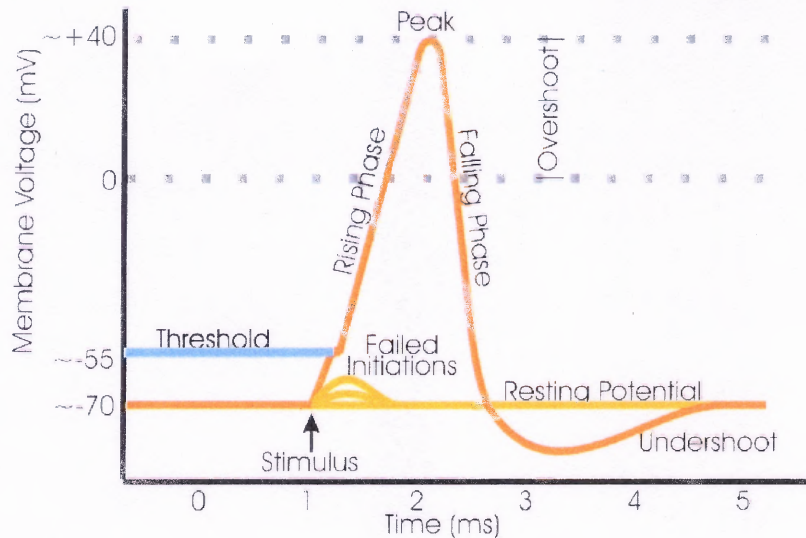
Figure 2.2 General characteristics of an action potential. Reprinted by permission under the terms of the GNU Free Documentation License (No author, 2005).

follows, it is more difficult to initiate another action potential because the sodium channels only slowly recover from inactivation.

Once a patch of membrane is depolarized by inward sodium current, the positive charge diffuses laterally to the adjacent areas and depolarizes the membrane. In regions which have not been excited before, the sodium channels are not inactive and therefore open and restore the action potential. The action potential, once initiated, e.g. at the axon hillock, travels down the axon at a speed of up to 1cm/ms or higher (Koch, 1999). It will never reverse, since the region just activated cannot be activated again because of the refractory period.

For each single cell the action potential has a stereotypical shape that does not reflect the type or duration of the input but is an all-or-nothing event. A variety of shapes can be observed in different cell types, and the peak lasts one to two milliseconds, dependent on the temperature (Koch, 1999). The time course of a typical action potential is shown in Figure 2.2. Important to note is that the changes in concentration of potassium and sodium ions in the external and internal solutions during the action potential are extremely small (Hodgkin and Huxley, 1952).

If the threshold is not reached, only a slight depolarization can be observed and the membrane potential quickly returns to its resting value. The spread of a so called localized graded potential depends on the passive properties of the nerve cell. The graded potential usually does not travel far because it is not restored in amplitude.

2.3 Electrical Synapse

In the last section signal generation and transmission within a single neuron has been discussed. However, neurons are not separate units but connect to one another by chemical or electrical synapses in order to conduct electrical signals. The role of electrical synapses was controversial for a long time but is now accepted to offer a second major pathway in addition to chemical synapses in signal conductance (Hormuzdi et al., 2004; LeBeau et al., 2003; Zoidl and Dermietzel, 2002).

Electrical synapses occur at gap junctions that connect the cytoplasm of two adjacent neurons by intercellular channels. A few to over 10^5 channels contribute to a gap junction (Simon and Goodenough, 1998). Each channel in the cluster has an internal pore of about 1.2nm in diameter, which allows ions, second messengers such as inositol triphosphate (IP3) or cyclic adenosine monophosphate (cAMP), and other small molecules up to a molecular weight of 1kDa to pass from one cell to the other (Bennett and Zukin, 2004; Hormuzdi et al., 2004). At the gap junction, the membranes of the two neurons are only 2-4nm apart (Hormuzdi et al., 2004).

The proteins forming the gap junction have been characterized on the molecular level. For the gap junction each neuron contributes a 7nm long hemichannel (connexon), which consists of six proteins called connexins in vertebrates. At least 20 different connexins have been identified in the human genome (Zoidl and Dermietzel, 2002). Based on their molecular weight in kDa, the connexins are called Cx36, Cx43, and so on. The connexins differ in their permeability, their gating procedure, transcriptional regulation, and degradation (Bennett and Zukin, 2004).

In most cases, gap junctions are established between two neurons of one class, inter-neurons, for example (LeBeau et al., 2003; Beierlein, Gibson, and Connors, 2000; Gibson, Beierlein, and Connors, 1999). The location of the gap junction varies greatly: Dendro-dendritic, dendro-somatic, and axo-axonal gap junctions have been identified (LeBeau et al., 2003; Fukuda and Kosaka, 2003; Traub et al., 2001; Zoidl and Dermietzel, 2002; Traub et al., 2003).

The ionic current between the two electrically coupled cells is a result of the electro-chemical gradient and is mostly carried by potassium ions (Bennett and Zukin, 2004). In the case of a symmetric gap junction, the current flows equally well in both directions. In contrast, rectifying gap junctions gate the ionic flux dependent on the potential of the cells. The symmetric gap junction acts as a low-pass filter, and the postsynaptic response is attenuated relative to the presynaptic signal (Gibson, Beierlein, and Connors, 1999). If the presynaptic cell is depolarized compared to the coupled cell, the current flows into the coupled, postsynaptic cell and first charges the capacitor before changing the membrane potential. When the presynaptic cell repolarizes the current reverses direction and damps the postsynaptic potential.

In humans numerous electrical synapses have been detected in the neocortex, the hippocampus, the locus coeruleus, the retina, and other parts of the brain (LeBeau et al., 2003; Zhang and Poo, 2001). Cx36 is widely expressed, and it has been proven relevant for the generation and mediation of widespread, synchronous inhibitory activity (Zoidl and Dermietzel, 2002). Oscillations are assumed to be important in behavior, memory, sensory perception, motor activity, and learning (LeBeau et al., 2003; Hormuzdi et al., 2004). Traub et al. (2001) outlined the possible importance of axo-axonal gap junctions in the generation of very fast oscillations before seizure onset in principal neurons. Besides, axo-axonal gap junctions have been found to mediate high-frequency oscillations, and they have been attributed to generate fast oscillations in pyramidal cells (Zoidl and Dermietzel, 2002; Traub et al., 2003).

For many years the high speed of transmission has been pronounced as the main characteristic of electrical synapses. In contrast to chemical synapses, where it takes about

1-5ms for the signal to arrive at the postsynaptic cell, the conductance at the electrical synapse is almost instantaneous (Kandel, Schwartz, and Jessell, 2000). The detection of electrical synapses in escape mechanisms, where quick responses are crucial, seems an immediate consequence (Kandel, Schwartz, and Jessell, 2000). Considering that the higher body temperature reduces the delay at chemical synapses, the speed of electrical signal transmission in mammals is not as fundamental as in cold-blooded animals (Bennett and Zukin, 2004). However, the temporal synchronization of action potentials is significant in the heart, for example, where it ensures the coordinated contraction of the cardiac myocytes (Simon and Goodenough, 1998). Synchronization is a result of both the electrical coupling and the biochemical communication between the cells. Kandler and Katz (1998) suggested that neuronal activity is coordinated partially by communication via second messengers such as Ca^{2+}. The coupling strength plays an important role in the degree of synchronization. Marder (1998) found that weak coupling between neurons can decrease synchrony resulting in out-of-phase firing.

Conducting subthreshold signals into the postsynaptic cell is characteristic of gap junctions and is important for the network behavior (Beierlein, Gibson, and Connors, 2000). In the retina, the interaction of electrically coupled cells reduces the noise and therefore improves the resolution (Bennett and Zukin, 2004; Hormuzdi et al., 2004).

In the developing central nervous system chemical synapses are not widely spread and furthermore immature. Gap junctions are abundant and they are assumed to be important for axonal guidance during the formation of neuronal circuits. Calcium ion flux between two electrically coupled neurons is crucial since Ca^{2+} transients are involved in modulating nerve growth and stimulating differentiation of nerve cells (Zhang and Poo, 2001). The number of gap junctions is reduced during adolescence and the persistent gap junctions are refined (Hormuzdi et al., 2004).

In general, electrical and chemical synapses coexist and are sometimes interrelated in form of "mixed synapses" (Mamiya, Manor, and Nadim, 2003). Fukuda and Kosaka (2003) detected the chemical synapse in hippocampal neurons to generate oscillatory activity and the electrical synapse to maintain synchrony.

Until recently, electrical synapses have been assumed to lack plasticity. In contrast, modulation of the absolute number of expressed channels as well as diversity with respect to the conductance of single channels has been proven. Landisman and Connors (2005) showed a temporal reduction of the electrical synapse's strength in mammalian neurons experimentally, and assumed that long-term potentiation exists as well. Phosphorylation of connexins and intracellular Ca^{2+} levels may regulate and mediate coupling strength (Bennett and Zukin, 2004; Koch, 1999). Some chemical agents affect gap junctions, and acidic pH levels have been proven to uncouple cells (Kandel, Schwartz, and Jessell, 2000; Nicholls et al., 2001; LeBeau et al., 2003; Hampson, Weiler, and Vaney, 1994; Zoidl and Dermietzel, 2002).

The efficacy of the electrical synapses crucially depends on the properties of both neurons, as well as the resistance of the gap junction. The impact of the coupling strength has been examined by Sharp, Abbott, and Marder (1992) using an artificial electrical synapse. In a theoretical study Nadim and Golowasch (2006) recently examined the effect of the connected fibers' diameters and found that the amplitude of the postsynaptic potential is maximized for a specific diameter in the postsynaptic cell. The optimal diameter arises as a result of two opposing characteristics. On the one hand, the length constant increases with diameter resulting in a decreased voltage attenuation along the neuronal process. On the other hand, the gap junction acts as a current limiter which leads to a lower current density in the coupled cell for a fiber of larger diameter. In this thesis, the influence of the diameter on the initiation of an action potential and its propagation in two electrically coupled neurons is examined, and the application to networks of neurons is demonstrated.

CHAPTER 3

MODELING THE NERVOUS SYSTEM

Theoretical and computational models of single or interconnected neurons provide a tool to better understand the nervous system and how it functions. In situations where wet-bench experiments are not feasible, effects of changing characteristics of the neurons or their connectivity can be examined. Additionally, computer simulations help to confirm results of experiments.

This chapter is dedicated to understanding how the properties of neurons discussed in Chapter 2 can be modeled. The complexity of a neuronal model depends on the accuracy of the geometrical and electrical representation and has to be adjusted to the needs of the study. Here, the geometry of the neuron is approximated by a compartment model and the membrane's complexity is reduced to the cases of passive and excitable Hodgkin-Huxley-like membranes.

First, a continuous representation of the temporal and spatial potential distribution in a thin, elongated neuronal structure with passive membrane properties is given, which is based on the concepts of the linear cable theory. However, exact solutions of the partial differential equation are restricted to the case of a membrane without voltage-dependent characteristics. Therefore, compartmental modeling is introduced in Section 3.2. In this approach, the neuronal structure is broken into discrete, isopotential segments. This transforms the partial differential equation into a system of ordinary differential equations. In order to include nonlinear, voltage-gated properties of excitable membranes, the Hodgkin-Huxley model is discussed in Section 3.3 and incorporated into the compartment representation.

3.1   Linear Cable Theory

Cable theory describes the conductance of electrical signals along cables. This theory can be applied to study signal transmission in neurons. The semipermeable membrane,

which separates the extracellular fluid from the cytoplasm, acts as a capacitor, and ion channels penetrating the membrane can be modeled by resistors. The electrochemical gradients established by the selective permeability of the membrane and maintained by ion pumps and transporter molecules can be compared to a battery. The cytoplasm and the extracellular fluid are ionic solutions that conduct electrical current and can be represented by resistors. However, the intracellular fluid is about 10^7 times worse than a metal wire in transmitting signals because the density of ions in the cytoplasm is much lower than the density of free electrons in wires (Nicholls et al., 2001). Additionally, because the membrane is not a perfect insulator, current is lost by outward leakage and signals are attenuated quickly.

Modeling parts of a neuron as a passive cable, the membrane properties are assumed to be constant and the channels to be independent of voltage, time, ligands or second messengers. Obviously, this is a simplification, since not only axons but also dendrites have been shown to exhibit voltage-dependent behavior (Saraga et al., 2003; Johnston et al., 2003; Cook and Johnston, 1999). However, experimental data suggests that parts of the neuron conduct signals indeed passively (Keener and Sneyd, 2001). Besides, the distribution and density of active channels in dendrites is unknown. This motivates the work on passive structures both as benchmark systems and as a step to understanding the more complicated case of excitable membranes (Koch and Segev, 1998).

A simple geometric structure that represents parts of the axon or dendrite is a cylinder. Using linear cable theory, it can be simulated how an electrical signal traveling down a cable-like structure is delayed and distorted when it arrives at the soma.

3.1.1 Cable Equation

Dendrites are often assumed to behave like one-dimensional cables, transmitting incoming impulses passively and only in the longitudinal direction. A dendrite modeled as a passive cable can be approximated by an electrical circuit as shown in Figure 3.1, where each RC circuit element represents an isopotential patch of membrane of length Δx. The membrane is characterized by a capacitance c_m ($\frac{F}{cm}$) in parallel to a voltage-independent resistance
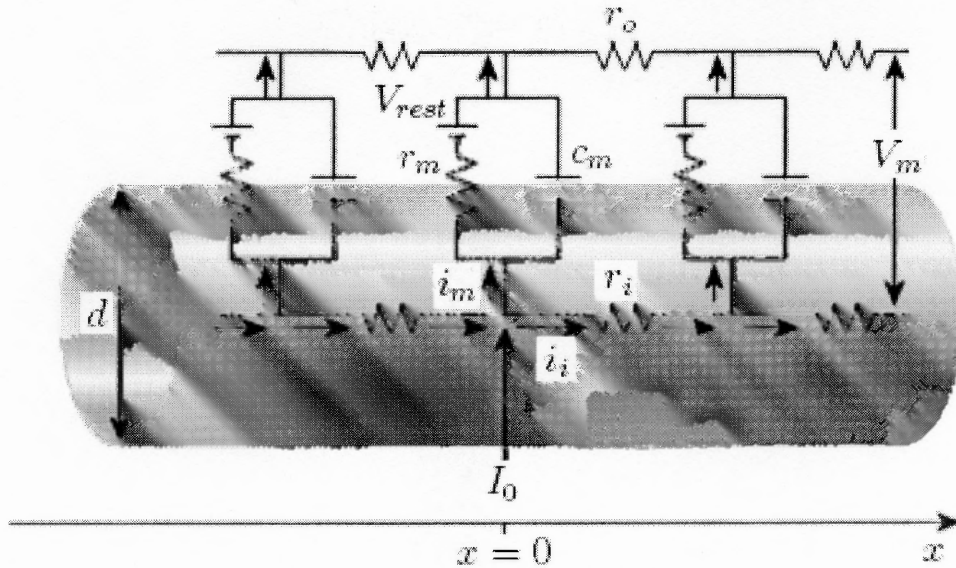
Figure 3.1 Schematic diagram of the current flow in a passive, cylindrical dendrite and the corresponding electrical circuit superimposed.

r_m (Ωcm) and a battery V_{rest}. The cytoplasm and the extracellular fluid are represented by a longitudinal intracellular resistance r_i ($\frac{\Omega}{cm}$) and an extracellular resistance r_o ($\frac{\Omega}{cm}$), respectively.

The cable equation

$$\lambda^2 \frac{\partial^2 V(x,t)}{\partial x^2} = \tau \frac{\partial V(x,t)}{\partial t} + V(x,t) \tag{3.1}$$

describes the voltage distribution in a one-dimensional cable. $V(x,t)$ is the transmembrane potential which is defined relative to V_{rest} as

$$V(x,t) = V_m(x,t) - V_{rest}.$$

$\lambda = \sqrt{\frac{r_m}{r_i}}$ is the length constant, and $\tau = c_m r_m$ is the time constant of the cable.

Measuring x and t in units of the length and time constant, $X = x/\lambda$, $T = t/\tau$, Equation (3.1) is simplified to

$$\frac{\partial^2 V(X,T)}{\partial X^2} - \frac{\partial V(X,T)}{\partial T} - V(X,T) = 0. \tag{3.2}$$

r_i, r_m and c_m are values for one centimeter of cable. In order to compare the membrane and intracellular properties of cells of different size and shape, the geometry independent parameters R_i (Ωcm), R_m (Ωcm^2) and C_m ($\frac{F}{cm^2}$), being the specific intracellular resistance, the specific membrane resistance, and the specific membrane capacitance respectively, are utilized. In relation to the cable parameters, they are defined as

$$R_i = \frac{1}{4}\pi d^2 r_i, \tag{3.3}$$

$$R_m = \pi d r_m, \tag{3.4}$$

$$C_m = \frac{c_m}{\pi d}, \tag{3.5}$$

where d is the diameter of the cable in centimeters. For the length and the time constant

$$\lambda = \sqrt{\frac{R_m d}{4R_i}}, \tag{3.6}$$

$$\tau = C_m R_m,$$

follows.

Solutions of the cable equation are functions dependent on time and space. In order to solve the equation for a special case, boundary conditions have to be specified. Here, an analysis of the steady-state solution of the cable equation is performed. Although at synapses input is transient, the steady-state solution often serves as an important reference and, especially in the case of high-frequency input, approximates the solution well (Koch and Segev, 1998).

In the steady-state, the voltage does not change with time, thus

$$\frac{\partial V}{\partial T} = 0, \text{ for } T \to \infty.$$

This reduces (3.2) to an ordinary differential equation

$$\frac{d^2 V(X, \infty)}{dX^2} = V(X, \infty). \tag{3.7}$$

The general solution of (3.7) reads

$$V(X, \infty) = A_1 e^X + A_2 e^{-X} = B_1 \cosh(L - X) + B_2 \sinh(L - X).$$
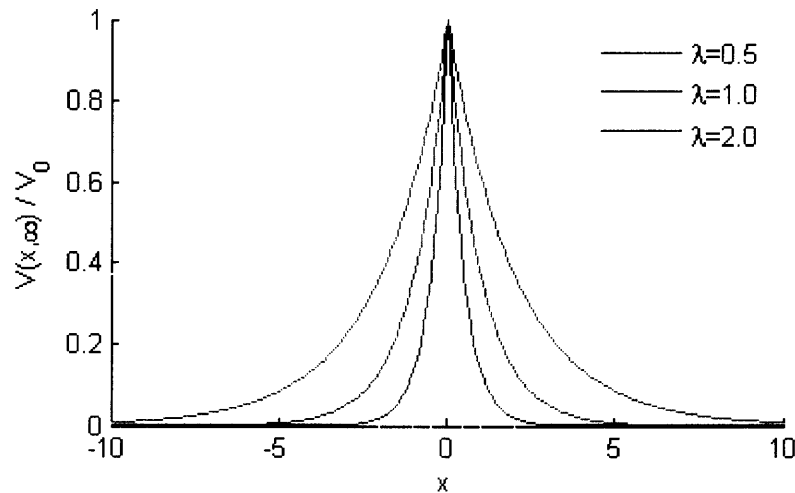
Figure 3.2 Relative potential attenuation along an infinite cable as a function of distance x from the point of voltage clamp $x = 0$, for different length constants λ.

In the following, two special cases of the steady-state solution are discussed. The case of the infinite cable provides a physical interpretation of the length constant λ and introduces the input resistance R_{in}. A finite cable with leaky boundary conditions can be used to model a passive dendrite that is gap junctionally coupled to a target neuron.

3.1.2 Infinite Cable

Clamping the voltage at $V = V_0$ at the position $X = 0$ of the cable provides a boundary condition for the case of an infinite cable. The solution of the cable equation for the infinite cable is given by

$$V(X, \infty) = V_0 e^{-|X|} \quad \Leftrightarrow \quad V(x, \infty) = V_0 e^{-\frac{|x|}{\lambda}}.$$

The voltage decays exponentially with distance from the site of the voltage clamp, as illustrated in Figure 3.2. The length constant λ describes the attenuation of the voltage: At $|x| = \lambda$ the voltage has decreased to 37% of the initial value V_0 (see Figure 3.2). As seen in Equation (3.6), the length constant is proportional to the square root of the diameter. Cables that are longer than three length constants are assumed to be infinite. A dendrite

is usually about one length constant long. Therefore, the dendrite has to be modeled as a finite cable, which is discussed in Section 3.1.3.

The current I_0, which has to be applied at $x = 0$ to maintain the voltage at its desired value V_0, is dependent on the input resistance of the cable

$$R_{in} = \frac{V(0, \infty)}{I_0} = \frac{V_0}{I_0}.$$

The definition of the input resistance holds for cells of every shape and represents an average resistance of the intracellular fluid and the membrane to the applied current. The input resistance of an infinite cable is given by

$$R_{in} = \frac{r_i \lambda}{2} = \sqrt{\frac{R_m R_i}{d^3 \pi^2}}.$$

In the case of a semi-infinite cable that is sealed at $x = 0$, so that no current can flow to the direction of decreasing x

$$R_\infty = 2\sqrt{\frac{R_m R_i}{d^3 \pi^2}} \tag{3.8}$$

follows for the input resistance R_∞.

3.1.3 Finite Cable

Because neurons have an axon and dendrites of finite length that fall in the order of one length constant, the cable equation for a cable of a finite length len is outlined in this section.

Expressing len in units of the length constant, $L = \frac{len}{\lambda}$, the voltage at position X can be calculated as

$$V(X, \infty) = V_0 \frac{\cosh(L - X) + \frac{R_\infty}{R_T} \sinh(L - X)}{\cosh(L) + \frac{R_\infty}{R_T} \sinh(L)}, \tag{3.9}$$

where R_∞ is the input resistance of a semi-infinite cable, and R_T represents the terminating resistance of the finite cable. The input resistance of a finite cable is given by

$$R_{in} = R_\infty \frac{1 + \frac{R_\infty}{R_T} \tanh(L)}{\frac{R_\infty}{R_T} + \tanh(L)}.$$

Modeling a finite cable with leaky end, the terminating resistance is set to the appropriate value $R_T < \infty$. A sealed end at $X = L$ corresponds to $R_T = \infty$. Using Equation (3.9) one can simplify the solution to

$$V(X, \infty) = V_0 \frac{\cosh(L - X)}{\cosh(L)}.$$

For the input resistance follows $R_{in} = R_\infty \coth(L)$.

3.2 Compartmental Modeling

Representing the neuron by discrete, interconnected, isopotential compartments transforms the partial differential equation for the potential into a system of ordinary differential equations. Voltage-dependent membrane properties that cannot be modeled using linear cable theory and nonuniform characteristics in different parts of the cell can be included into the compartment model.

Dividing the neuron into several segments of short length (rule of thumb: $< \frac{\lambda}{10}$), it is assumed that the compartments are isopotential and uniform in their properties (Koch and Segev, 1998). The segments are interconnected by a resistor that resembles half of the intracellular resistance of the adjacent cells. Differences in membrane properties, diameter, or voltage occur between the compartments instead of within them. The so called "equivalent cylinder" of a neuron similar to that in Figure 2.1 is shown in Figure 3.3.

For each segment j the incoming and outgoing currents have to balance

$$i_{m\,j} = I_{ext\,j} + i_{j-1,j} - i_{j,j+1}.$$

$i_{m\,j}$ is the membrane current, $i_{j-1,j}$ is the current between segments $j - 1$ and j, and $I_{ext\,j}$ denotes a current applied to compartment j. Expressing the axial current in terms of the difference in transmembrane voltage between the adjacent segments, and separating the membrane current into its capacitive and ionic components, one gets

$$c_m^{(j)} \frac{dV_j}{dt} = -I_{ion\,j} + I_{ext\,j} + \frac{V_{j-1} - V_j}{r_{j-1,j}} - \frac{V_j - V_{j+1}}{r_{j,j+1}}.$$

(a)   (b)
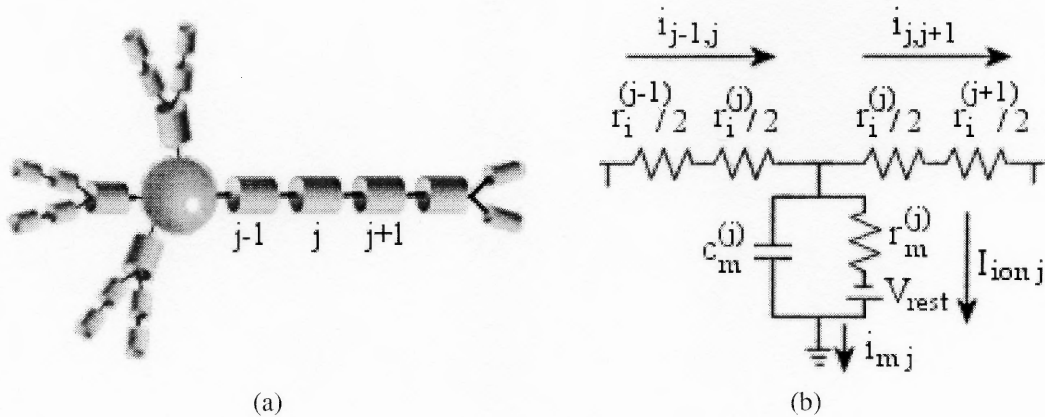
Figure 3.3 (a) Equivalent cylinder representation of a neuron. Each segment is assumed isopotential and exhibits uniform passive membrane properties. (b) Electrical circuit representation for segment j. The extracellular resistance is taken as zero. The membrane resistance is represented by the resistor $r_m^{(j)}$ and the membrane capacitance by $c_m^{(j)}$. The membrane current $i_{m\,j}$ is the sum of the capacitive and the ionic current. The intracellular resistance between segment $j-1$ and segment j is $\frac{r_{j-1}+r_j}{2}$. The longitudinal current through this resistance is denoted $i_{j-1,j}$.

The ionic current $I_{ion\,j}$ across the membrane of segment j can be a linear leak current as implied in Figure 3.3. However, this term can also describe complex nonlinear properties of ion channels, which may be different from segment to segment. Channels controlled by chemical agents such as second messengers or neurotransmitters, as well as time-dependent behavior can be modeled. In the following section the Hodgkin-Huxley model, which describes the properties of excitable membranes in terms of voltage-dependent ionic flux, is introduced.

3.3   Hodgkin-Huxley Model

The mechanisms of action potential initiation and propagation have been studied by a number of researchers. Using data derived from voltage clamp experiments on the squid giant axon, Hodgkin and Huxley (1952) described the action potential generation in terms of four differential equations that represent the ionic flux across the cell membrane through selective, voltage-gated ion channels. Their research resulted in a shared Nobel Prize in Physiology or Medicine in 1963. Duration and amplitude of the action potential, as well as the conduction velocity, ionic movements and subthreshold phenomena fit the experimental

data well. The form of the action potential is reconstructed except for the rise at the start of the action potential (Hodgkin and Huxley, 1952). Throughout the model it is assumed that the concentration of the extracellular fluid is constant and that the volume of the cell does not change.

In a number of experiments, Hodgkin and Huxley (1952) identified potassium and sodium currents to be the major currents in the generation of action potentials. The time- and voltage-dependent conductance of the membrane to these ions, G_K and G_{Na}, is modeled by dimensionless gating variables, which represent the fraction of open channels. The transition between the open and closed states is assumed to follow first-order kinetics.

The gating variable for the potassium channel $n = n(V_m, t)$ solves the differential equation

$$\frac{dn}{dt} = \frac{n_\infty(V_m) - n}{\tau_n(V_m)},$$

with the time constant $\tau_n(V_m)$ and the steady-state activation curve $n_\infty(V_m)$.

The total number of open K^+ channels at a specific voltage and time is equivalent to the product of $n(V_m, t)^4$ and the maximum conductance $\bar{g}_K$. $n(V_m, t)$ was raised to the power of four in order to fit the data. However, one may assume that the movement of four independent particles is required for the channel to change into its open state.

Hodgkin and Huxley (1952) discovered that the sodium conductance is characterized by two independent processes, a rapid, almost instantaneous sigmoid activation and a slower, exponential inactivation. The voltage-dependent gating variables $m = m(V_m, t)$ for the activation, and $h = h(V_m, t)$ for the inactivation are derived analogical to the gating variable of the potassium current as

$$\begin{aligned}
\frac{dm}{dt} &= \frac{m_\infty(V_m) - m}{\tau_m(V_m)}, \\
\frac{dh}{dt} &= \frac{h_\infty(V_m) - h}{\tau_h(V_m)}.
\end{aligned}$$

In order to fit the experimental data, m has to be raised to the power of three and multiplied by h and $\bar{g}_{Na}$, which is the maximal conductance of the sodium channels.
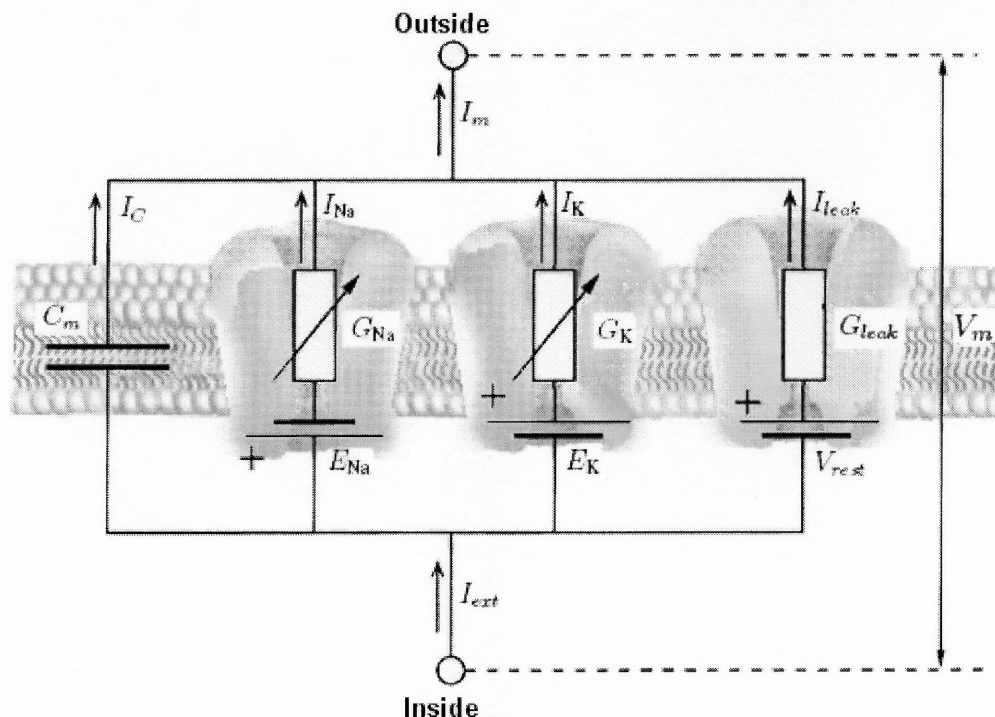
Figure 3.4 Hodgkin-Huxley Model: Circuit representation of the current flow for a patch of membrane.

The passive flux of chloride ions across the membrane, as well as currents carried by ion pumps and transporters are represented by the time- and voltage-independent variable I_{leak}.

For a piece of membrane as illustrated in Figure 3.4, the membrane potential V_m can be calculated by solving the nonlinear differential equation

$$
\begin{aligned}
C_m \frac{dV_m}{dt} &= I_{ext} - I_{leak} - I_{Na} - I_K \\
&= I_{ext} - G_{leak}(V_m - V_{rest}) - \bar{g}_{Na}m^3 h(V_m - E_{Na}) - \bar{g}_K n^4(V_m - E_K),
\end{aligned}
$$

with m, h, n defined by the linear first-order differential equations given above.

The membrane patch modeled here can be incorporated into the compartment model described in Section 3.2 by replacing $I_{ion\ j}$ for each compartment j with the ionic current given by the Hodgkin-Huxley equations. The time evolution of the compartmentalized model can then be simulated by integrating the rate and voltage equations numerically.

3.4 Modeling an Electrical Synapse

Studying a network of neurons means studying the impact of one neuron on its intercon-nected neurons. Two neurons can either be connected by chemical or electrical synapses, of which the latter is further examined in this thesis. As discussed in Section 2.3 ionic current I_{gj} between two neurons coupled by a symmetric gap junction depends on the potential difference between the two cells

$$I_{gj} = G_{gj}(V_{pre} - V_{post}),$$

where V_{pre} and V_{post} are the potentials of the pre- and the postsynaptic cell, respectively. G_{gj}, the conductance of the gap junction, may be influenced by several agents, but for reasons of simplicity is assumed to be constant. In literature, the gap junction conductance varies, but typically lies in the range 1-5nS (Fukuda and Kosaka, 2003; Gibson, Beierlein, and Connors, 1999; Traub et al., 2003).

From the computational point of view, the gap junction between two neurons can be modeled by simply connecting the two adjacent compartments of the cells with an axial resistance $R_{gj} = G_{gj}^{-1}$.

The voltage at the postsynaptic side of the gap junction V_{post_0} depends on the voltage at tips of the presynaptic fiber V_{pre_L}, the input resistance of the postsynaptic cell R_{in_post}, and the resistance of the gap junction R_{gj}. The current flux across the gap junction has to be equal and opposite to the current flux into the postsynaptic cell:

$$I_{gj} = I_{post\_0} \quad \Leftrightarrow \quad \frac{V_{pre\_L} - V_{post\_0}}{R_{gj}} = \frac{V_{post\_0}}{R_{in\_post}}.$$

For the voltage at the postsynaptic side of the gap junction

$$V_{post\_0} = \frac{R_{in\_post} V_{pre\_L}}{R_{gj} + R_{in\_post}} \tag{3.10}$$

follows.

CHAPTER 4

OPTIMAL DIAMETER IN SIGNAL TRANSMISSION

For neurons connected by gap junctions, Nadim and Golowasch (2006) detected a so called "optimal diameter" for which the postsynaptic potential (PSP) is maximal in amplitude. The existence of an optimal diameter implies that an action potential in the postsynaptic cell may only be initiated if the dendrite's diameter has the optimal value. The diameter of the coupled fiber therefore may contribute to the success or failure of synchronization and the generation of oscillations in neural networks.

Electrical coupling is prevalent in the mammalian brain, and dendro-dendritic gap junctions have been shown, e.g. in hippocampal and cortical neurons (Fukuda and Kosaka, 2003; LeBeau et al., 2003).

In this thesis, compartment models were built for the purpose of studying the influence of geometrical modifications on the signal transmission between two or more neurons which are gap junctionally coupled at their dendrites. The membrane and the cable equations were integrated numerically using the software Network, which is introduced in the following section. In Section 4.2, the investigated models of pairs of neurons are discussed, followed by a demonstration of the results in Section 4.3. Section 4.4 introduces models of a ring architecture of up to 10 neuron, and Section 4.5 presents the findings for this network study.

4.1   The Software

Network (`http://cancer.rutgers.edu/software/index.htm`) is a software that can be utilized to compute the voltage in the different segments of a compartment model. This command-line based simulation tool is implemented in C, and it was run under Cygwin in MS Windows.

As in most other programs for simulating neuronal activity, the morphology and the physical, chemical or electrical parameters are represented by two distinct data sets, a configuration and a parameter file (Koch and Segev, 1998). To calculate the solution of

the system of ordinary differential equations, a 4th-order Runge-Kutta method with a time step of 1μs was used.

4.2 Models of Two Coupled Neurons

A model reflecting the dendro-dendritic electrical coupling between two neurons was built. In several simulations the geometry of the neurons was varied, and its influence on the effectiveness of the signal transmission was examined. Of special interest was how the success or failure of action potential initiation is affected by the variation of the diameters of the coupled fibers.

First, the common features of the model-neurons are presented. Afterwards, each single model is introduced. In the following sections, the terms distal and proximal are used for locations on the neurites with the soma as a reference point.

4.2.1 General Assumptions about the Models

In order to approximate data from hippocampal basket cells, the passive properties of the cells were uniformly assumed to be $R_m = 40$ kΩcm^2, $R_i = 100$ Ωcm, and $C_m = 1$ μF/cm^2 (Saraga et al., 2003; Nadim and Golowasch, 2006). These choices resulted in

$$\tau = C_m R_m = 40\text{ms}.$$

The dendrites were assumed to be passive, leaky, 600μm long cables of different diameters, which were compartmentalized and approximated by linked, discrete cylinders of length $l = 100\mu$m. The segments were indexed from left to right (0 to 5), and the jth compartment of the dendrite of cell i was referred to as i_Dj.

To illustrate the calculations of the properties of the single compartments, a dendrite of diameter 10μm is considered: For the length constant of the cylinder $\lambda = 3162.3\mu$m follows with Equation (3.6). Using Equations (3.3) - (3.5) the intracellular resistance $\hat{r}_i$, the membrane resistance $\hat{r}_m$, and the membrane capacitance $\hat{c}_m$ for each cylinder of 100μm

length and 10μm diameter compute to

$$
\begin{aligned}
\hat{r}_i &= \frac{R_i}{A_c} \cdot l = \frac{4 \cdot 100\Omega\text{cm}}{\pi \cdot 10^{-6}\text{cm}^2} \cdot 10^{-2}\text{cm} = 1.27\text{M}\Omega, \\
\hat{r}_m &= \frac{R_m}{A_m} = \frac{4 \cdot 10^4\Omega\text{cm}^2}{\pi \cdot 10^{-5}\text{cm}^2} = 1.27\text{G}\Omega, \\
\hat{c}_m &= C_m \cdot A_m = 1\frac{\mu\text{F}}{\text{cm}^2} \cdot \pi \cdot 10^{-5}\text{cm}^2 = 31.4\text{pF},
\end{aligned}
$$

where A_c is the cross sectional area, and A_m is the curved surface area of the cylinder, which resembles the membrane. The conductance of the membrane to leak current, which is the inverse of the membrane resistance, is $\hat{g}_m = 0.785$nS. Similarly, the conductance between two segments is given by $\hat{g}_i = 785$nS. The properties of the cylinders were calculated for each diameter of the dendrites.

The soma of the cell was modeled by a sphere with a diameter of 20μm. Because the soma was assumed isopotential, the intracellular conductance was fixed to a high value ($\hat{g}_i = 20\mu$S). The membrane conductance and the membrane capacitance were calculated as above: $\hat{g}_m$=0.314nS, $\hat{c}_m$=12.6pF.

The voltage-dependent properties of the axon were approximated by a fast sodium current with instantaneous activation and delayed inactivation, a slow potassium current, and a leak current as described by the Hodgkin-Huxley kinetics (Section 3.3). The steady-state activation curves and time constants of the gating variables used in the simulations are given by

$$
m_\infty(V_m) = \frac{1}{1+e^{-\frac{x+40}{9}}}, \qquad \tau_m(V_m) = 0, \tag{4.1}
$$

$$
h_\infty(V_m) = \frac{1}{1+e^{\frac{x+62}{10}}}, \qquad \tau_h(V_m) = 1 + \frac{11}{1+e^{\frac{x+62}{10}}}, \tag{4.2}
$$

$$
n_\infty(V_m) = \frac{1}{1+e^{-\frac{x+53}{16}}}, \qquad \tau_n(V_m) = 1 + \frac{6}{1+e^{\frac{x+53}{16}}}. \tag{4.3}
$$

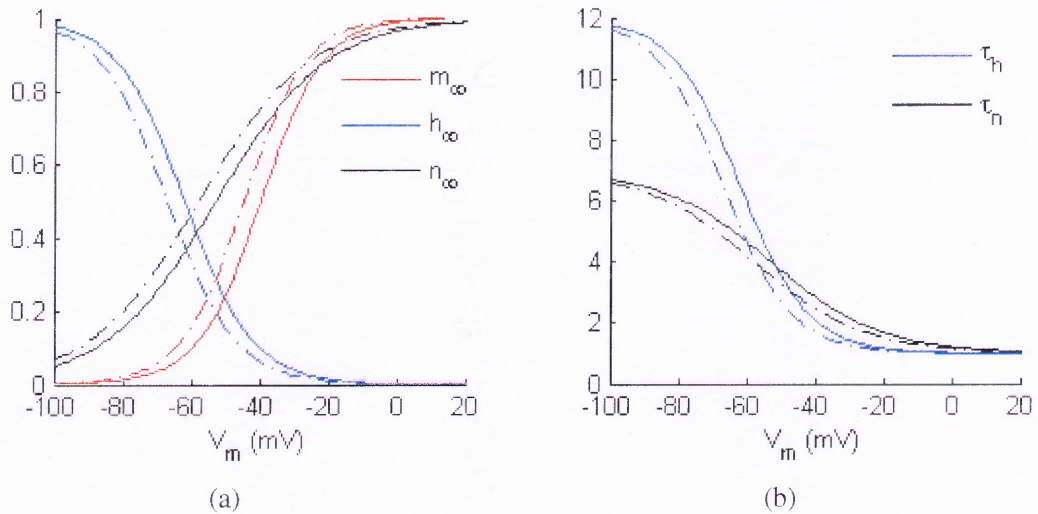The leak current in the voltage-dependent sections was represented by the passive membrane properties described above.

Figure 4.1 Steady-state activation curves and time constants of the two-gated sodium current and the single-gated potassium current. (a) m_∞ is the steady-state activation curve of the sodium current, h_∞ corresponds to the inactivation of the sodium current, and n_∞ describes the steady-state activation curve of the potassium channels. (b) The time constants for the inactivation of the sodium current (τ_h) and the activation of the potassium current (τ_n) are shown. The sodium current activation was assumed to be instantaneous ($\tau_m = 0$). The altered voltage-dependence of the steady-state activation curves and the time constants after reducing the threshold by 5mV is illustrated by the dash-dotted traces.

In all the simulations, the axon was 600μm long, had a diameter of 10μm , and was compartmentalized into six segments of equal length. The jth compartment of the axon of cell i was referred to as i_Aj, enumerating the segments from left to right.

Unless noted otherwise, two neurons were coupled at the tips of their dendrites via a symmetric gap junction with a conductance of G_{gj}=10nS.

The results of Nadim and Golowasch (2006) suggest that an action potential in the postsynaptic cell might be elicited only for an optimal diameter if the threshold is adequate. In order to investigate this, the threshold was varied by translating the activation curves and time constants of the sodium and potassium currents to lower values of the voltage. In Figure 4.1, the solid lines illustrate the steady-state activation curves and the time constants defined by Equations (4.1)-(4.3). The dash-dotted traces show the activation curves and time constants when the threshold for activation and inactivation was reduced by 5mV. In the following simulations, translating the activation curves and time constants of sodium and potassium currents to lower values is simply referred to as "reducing the threshold".
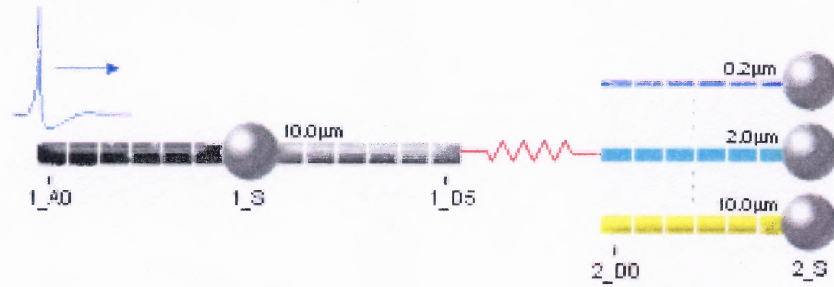
Figure 4.2 Schematic of the setup with a postsynaptic ball-and-stick neuron.

4.2.2 Postsynaptic Ball-and-Stick Neuron

The first model consisted of two neurons with different geometrical properties. Cell one was built connecting a spiking axon to a passive soma. A dendrite of length 600μm and diameter 10μm was connected to the soma. Cell two was designed as a 600μm long dendrite with a variable diameter $d = \{0.2\mu$m, 0.5μm, 1.0μm, 2.0μm, 5.0μm, 10.0μm$\}$, which was connected to a soma (Fig. 4.2). Every simulation was run with a different diameter of the dendrite of the postsynaptic ball-and-stick neuron. A similar model had been studied by Nadim and Golowasch (2006).

At t=20ms a current of 30nA was applied for 1ms to the distal compartment of the axon of cell one for the purpose of triggering an action potential.

4.2.3 Dendrite-and-Axon Model

In the second setup the previous ball-and-stick model of the postsynaptic cell was supplemented by an active, 600μm long axon with voltage-dependent properties (Fig. 4.3). The

Figure 4.3 Schematic of the dendrite-and-axon model. Every simulation was run with one postsynaptic dendrite-and-axon neuron.

Figure 4.4 Schematic of the multiple-dendrites model. Two cells with several dendrites were gap junctionally coupled at the tips of one single pair of dendrites.
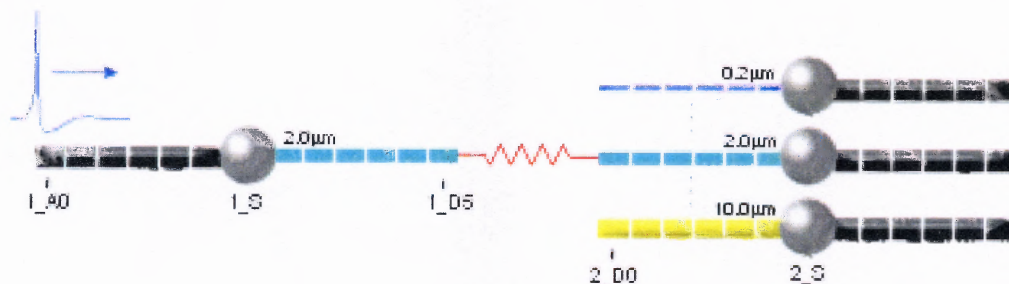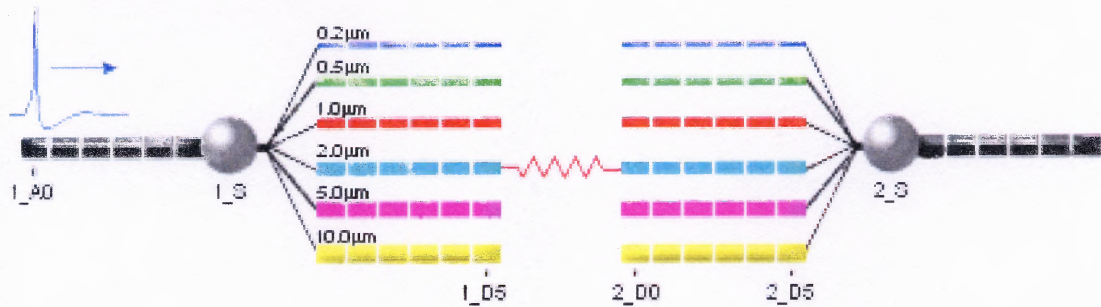
pre- and the postsynaptic dendrites' diameters were varied, and values in the range 0.1μm to 12μm were explored. No other changes were made.

An action potential was triggered by applying a current of 30nA for 1ms to the distal compartment of the presynaptic axon.

4.2.4   Multiple-Dendrites Model

In this more complex model two identical cells were generated, and each was made of an active axon, a passive soma, and six passive dendrites, which emerged from a node close to the soma. The dendrites had the diameters 0.2μm, 0.5μm, 1.0μm, 2.0μm, 5.0μm, and 10.0μm, respectively. In each simulation run, the cells were gap junctionally coupled at one pair of the dendrites that had the same diameter (Fig. 4.4).

At t=10ms a current of amplitude 3nA was applied for 2ms to the distal compartment of cell one, in order to initiate an action potential.

4.2.5   Partially-Active-Dendrites Model

In this scheme the presynaptic cell was simulated as a dendrite-and-axon neuron with a dendrite of diameter 5μm. The postsynaptic cell had several dendrites of the diameters $d =\{0.1\mu$m 0.2μm, 0.5μm, 1.0μm, 2.0μm, 5.0μm\}, a passive soma and an active axon. In contrast to the previous setups in which the dendrites were modeled as passive cables, the three proximal segments of the postsynaptic dendrites were equipped with voltage-gated
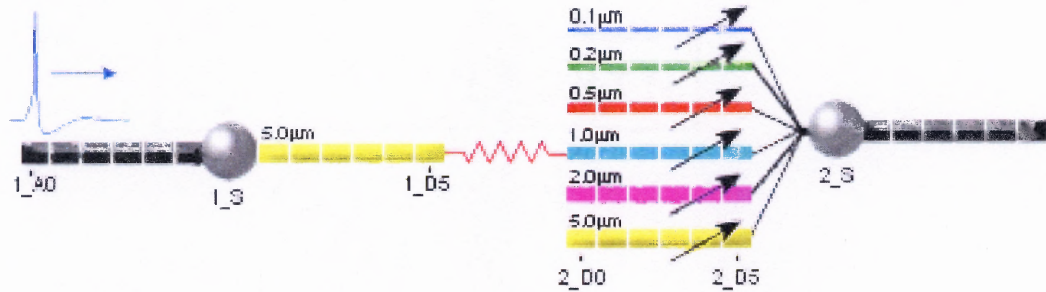
Figure 4.5 Schematic of the partially-active-dendrites model. The postsynaptic dendrites were equipped with voltage-gated properties in the proximal half, indicated by arrows.

ion channels (Fig. 4.5). In each simulation run the presynaptic dendrite was connected to one postsynaptic dendrite.

A current of 4nA was injected for 1ms into the distal compartment of the presynaptic axon for the purpose of triggering an action potential.

4.3   Results for Two Coupled Neurons

4.3.1   Postsynaptic Ball-and-Stick Neuron

The first goal was to assess the setup studied by Nadim and Golowasch (2006): Is spiking indeed initiated only in case the dendrite has the optimal diameter, presuming the threshold is apt?

The diameter of the postsynaptic dendrite was varied for all values indicated in Section 4.2.2 for the purpose of determinating the optimal diameter for the signal transmission. Figure 4.6a shows that a diameter of 2μm maximized the potential in the postsynaptic soma.

Subsequently, the soma was equipped with voltage-dependent properties to see if after adapting the threshold, an action potential could be triggered for the cell expressing the optimal diameter. Decreasing the threshold by 1mV resulted in an action potential for the neuron having a dendrite with the optimal diameter of 2μm. For a postsynaptic ball-and-stick neuron with a diameter different from the optimal value no action potential was initiated (Fig. 4.6b).

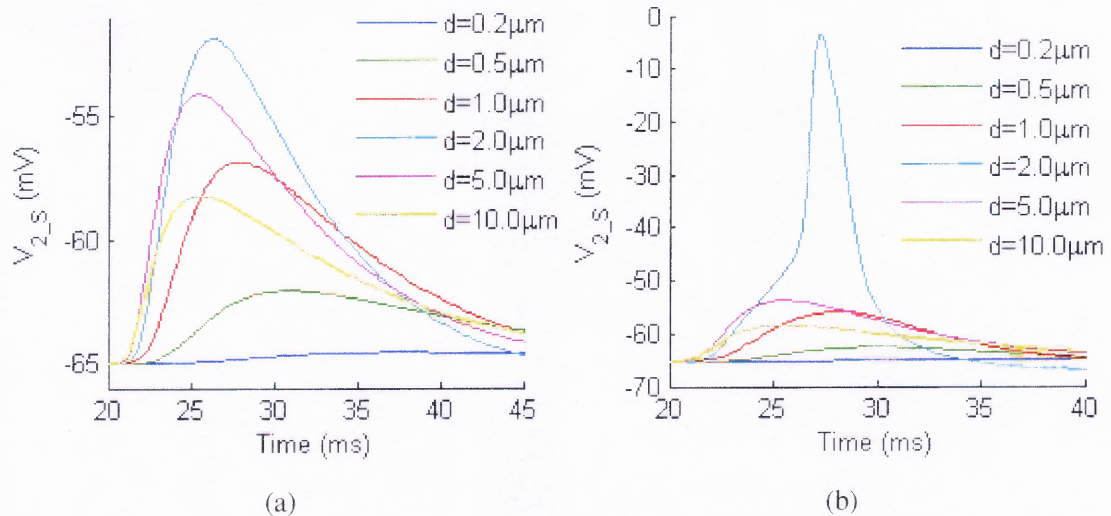**Figure 4.6** (a) The postsynaptic potential was optimized for a diameter of 2μm. (b) Making the postsynaptic soma active, and decreasing the threshold by 1mV an action potential was elicited when the dendrite had the optimal diameter.

4.3.2 Dendrite-and-Axon Model

Gap junctions are usually established between neurons of the same type (e.g. interneurons), and hence neurons of similar morphology. Therefore, studying gap junctions between two cells that are modeled symmetrically does not only simplify the model but is most of all biologically relevant.

Using the dendrite-and-axon model, the goal was again to investigate if an action potential is initiated only if the dendrite's diameter has the optimal value. Two different cases were examined. First, the diameters of both dendrites were varied simultaneously. Second, the diameter of only the postsynaptic dendrite was changed, while the diameter of the presynaptic dendrite was fixed.

When the diameters of both dendrites were varied simultaneously, the postsynaptic potential was maximized for $d = 8\mu$m (Fig. 4.7a). The optimal diameter was 2μm smaller when only the postsynaptic dendrite's diameter was varied and the diameter of the presynaptic dendrite was fixed to 8μm (Fig. 4.7b). This is in agreement with the observations made by Nadim and Golowasch (2006): A decreased voltage attenuation along the presynaptic dendrite decreases the optimal diameter. Since the length constant λ increases with
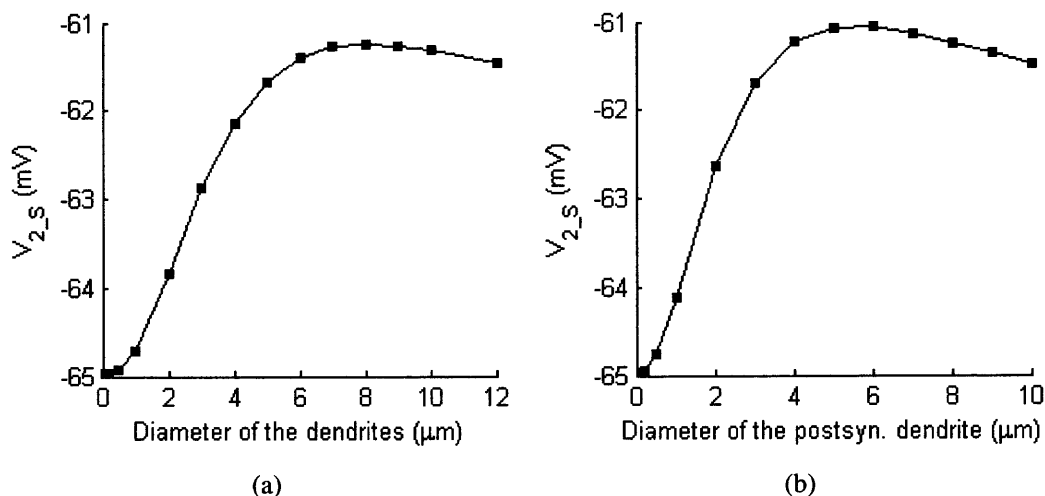
Figure 4.7 Peak voltage in the postsynaptic soma. (a) The diameters of both dendrites were varied simultaneously. The optimal diameter in this setup was 8μm. (b) The diameter of only the postsynaptic dendrite was varied. The potential was maximized for a diameter of 6μm.

the square root of the diameter of the fiber, a signal is more attenuated for a dendrite of a small diameter than for a thicker fiber.

Interestingly, when the threshold was decreased, the optimal diameter declined. A reduced threshold results in a larger number of open channels in the resting state, thus making the membrane more leaky. Nadim and Golowasch (2006) showed that the optimal diameter is lower if the membrane resistance is decreased, which may explain the observation made here.

In the case of a simultaneous variation of the dendrites' diameters, the threshold had to be reduced by at least 9.5mV in order to elicit an action potential. Translating the activation curves and time constants by 9.5mV, an action potential was generated when the diameter of the fibers was 5-6μm, thus smaller than the optimal diameter detected beforehand (Fig. 4.8a). For a larger diameter and for smaller diameters in the range 2μm to 4μm no action potential was triggered. When the diameter was further decreased to values smaller than or equal to 1μm, spontaneous spiking activity was observed (Fig. 4.8b).

When only the postsynaptic dendrite was varied, and when the threshold was reduced by 8.8mV, an action potential was triggered for a cell with a dendrite of diameter 4μm

(a)   (b)
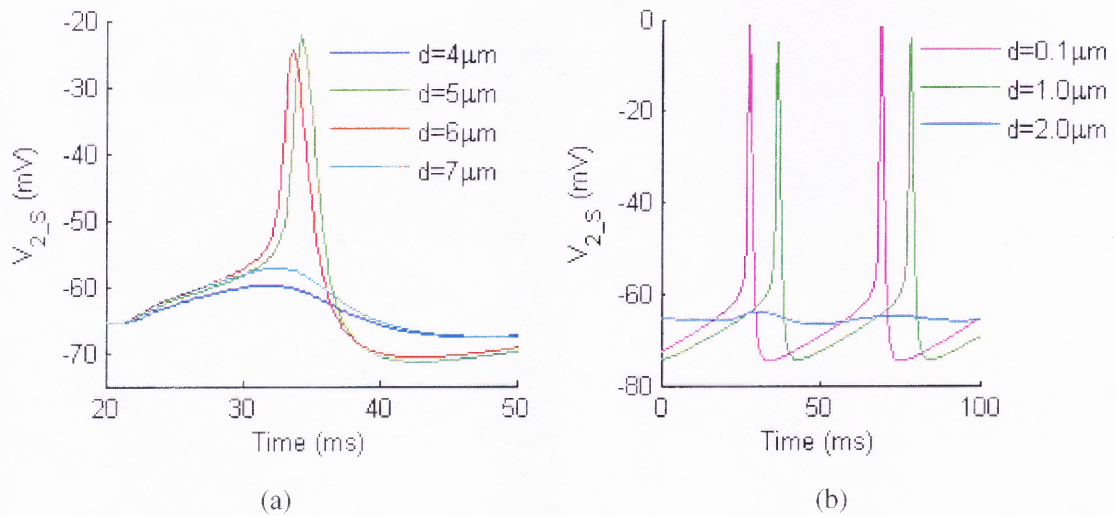
Figure 4.8 When the diameters of the dendrites were varied symmetrically, the threshold had to be reduced by 9.5mV in order to initiate an action potential. (a) An action potential was initiated for the diameters of 5μm to 6μm. There was no action potential for thicker dendrites, and for dendrites of a diameter of 2μm to 4μm . (b) For dendrites with a diameter $d \leq 1\mu$m spontaneous spiking was observed.

(a)   (b)

Figure 4.9 (a) When the threshold was reduced by 8.8mV, an action potential was triggered for a postsynaptic dendrite of diameter 4μm. For dendrites with a la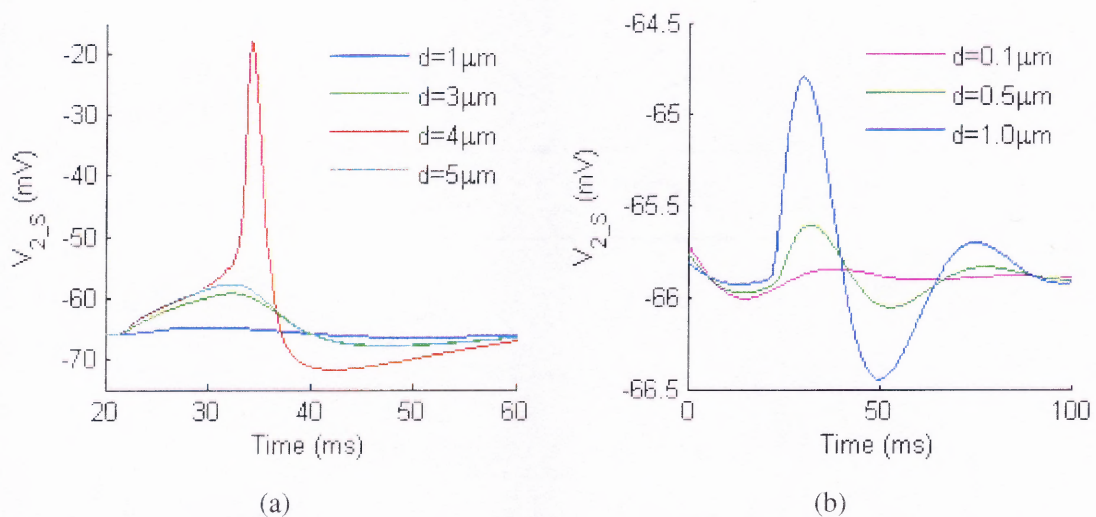rger diameter or a diameter of 2μm to 3μm, no action potential was initiated. (b) For dendrites of a diameter $d \leq 1\mu$m spontaneous, small-amplitude activity was observed.
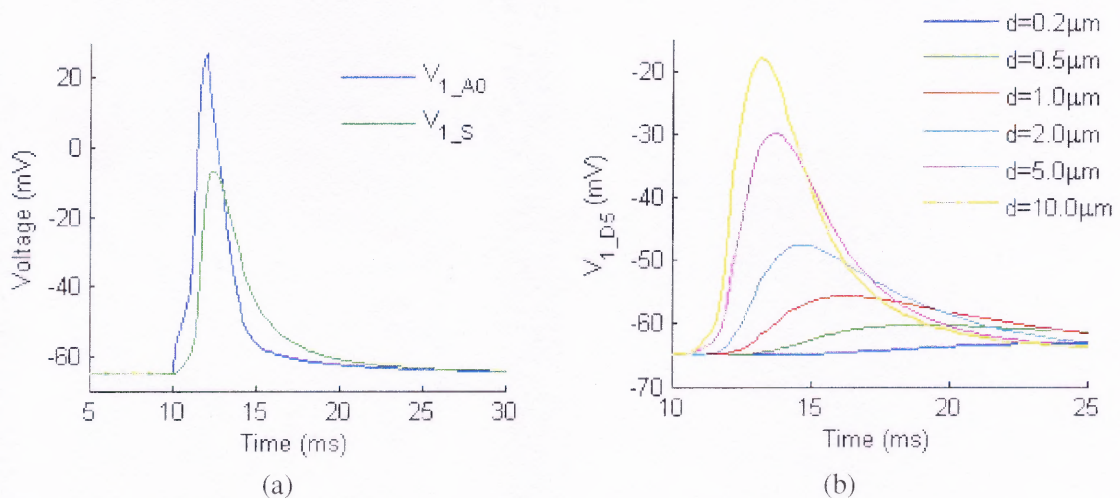
Figure 4.10 (a) Effect of the current injection to the distal compartment of the axon on the voltage in the axon and the voltage in the presynaptic soma. (b) Voltage measured at the tips of the dendrites of the presynaptic cell.

(Fig. 4.9a). This was again a lower value than the optimal diameter for this model. For dendrites with a larger diameter or a diameter of 2μm to 3μm, no action potential was triggered. However, as can be seen in Figure 4.9b spontaneous spiking activity, although small in amplitude, was prevalent for dendrites of diameters smaller than or equal to 1μm.

4.3.3 Multiple-Dendrites Model

The motivation for introducing a model with several dendrites (Fig. 4.4) was to control the spontaneous spiking activity of the model-neurons with dendrites of small diameter. The morphology of both neurons was kept identical for all operated simulations, and only the location of the gap junction was changed. This study resulted in the interesting observation that branching eliminates the optimal diameter.

For the multiple-dendrites model, the applied current initiated an action potential in the axon and caused a voltage of an amplitude of 60mV in the presynaptic soma (Fig. 4.10a). Because the presynaptic axon and soma were loaded by the six dendrites that emerged from a node close to the soma, the action potential lacked the undershot and the voltage in the soma was damped. As expected from the increasing length constant λ, the voltage atten-uation along the dendrites of the presynaptic cell decreased with the diameter (Fig. 4.10b). In contrast, the voltage drop across the gap junction increased with the diameter because
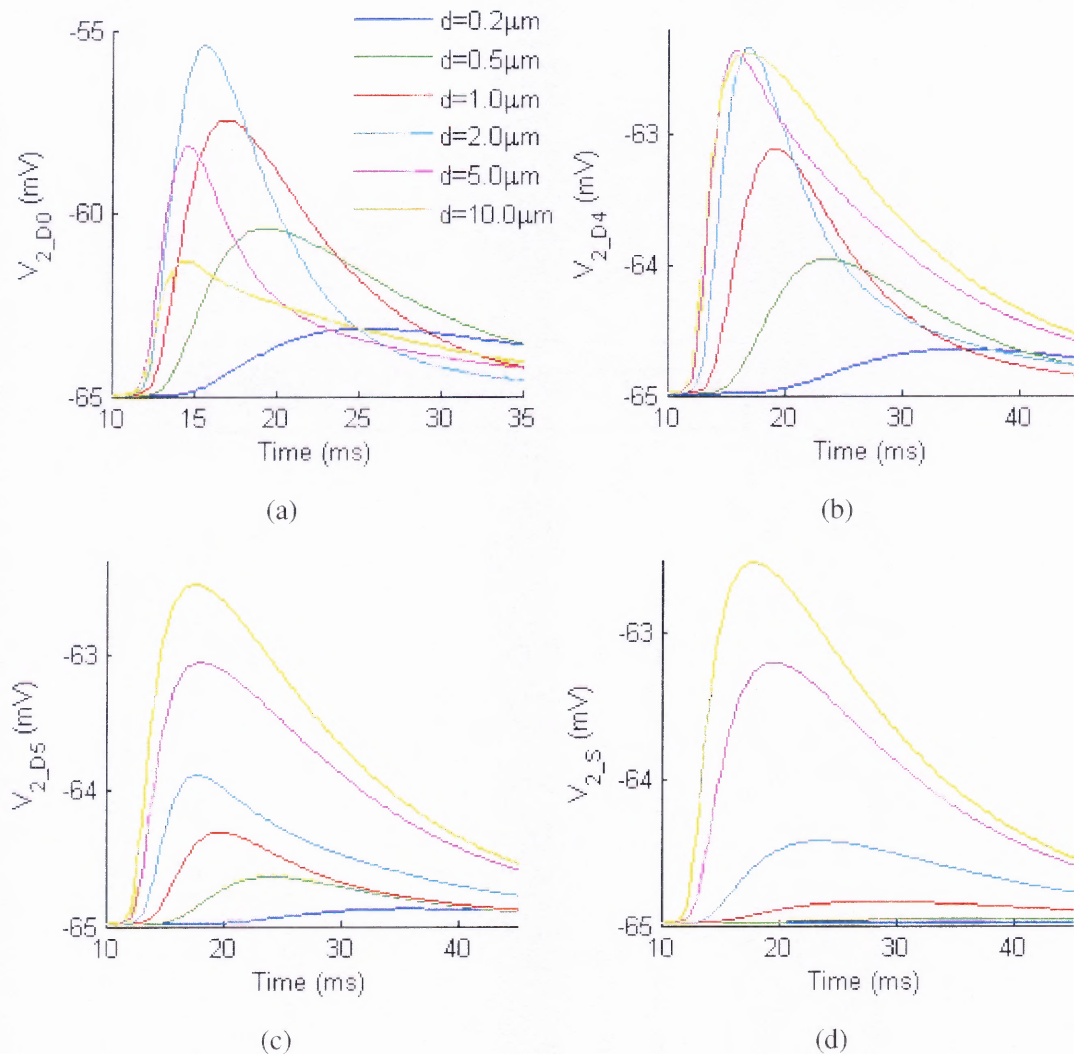
Figure 4.11 Potential at different locations of the postsynaptic cell in two neurons with several dendrites electrically coupled at the dendrites of diameter d.

the input resistance of the postsynaptic neuron decreased with the diameter of the postsynaptic fiber (see Equation (3.10)). These two opposing effects resulted in a potential of maximal amplitude for $d = 2\mu$m at the postsynaptic side of the gap junction, as illustrated in Figure 4.11a.

In the two proximal compartments of the postsynaptic dendrite and in the soma however, the voltage was damped, especially for the small diameters. This can be seen in Figure 4.11 by comparing the voltage in the fifth compartment of the dendrite (b) to the voltage in the sixth compartment (c) or the soma (d). In the last compartment and in the soma, the potential was an increasing function of the dendrite's diameter.
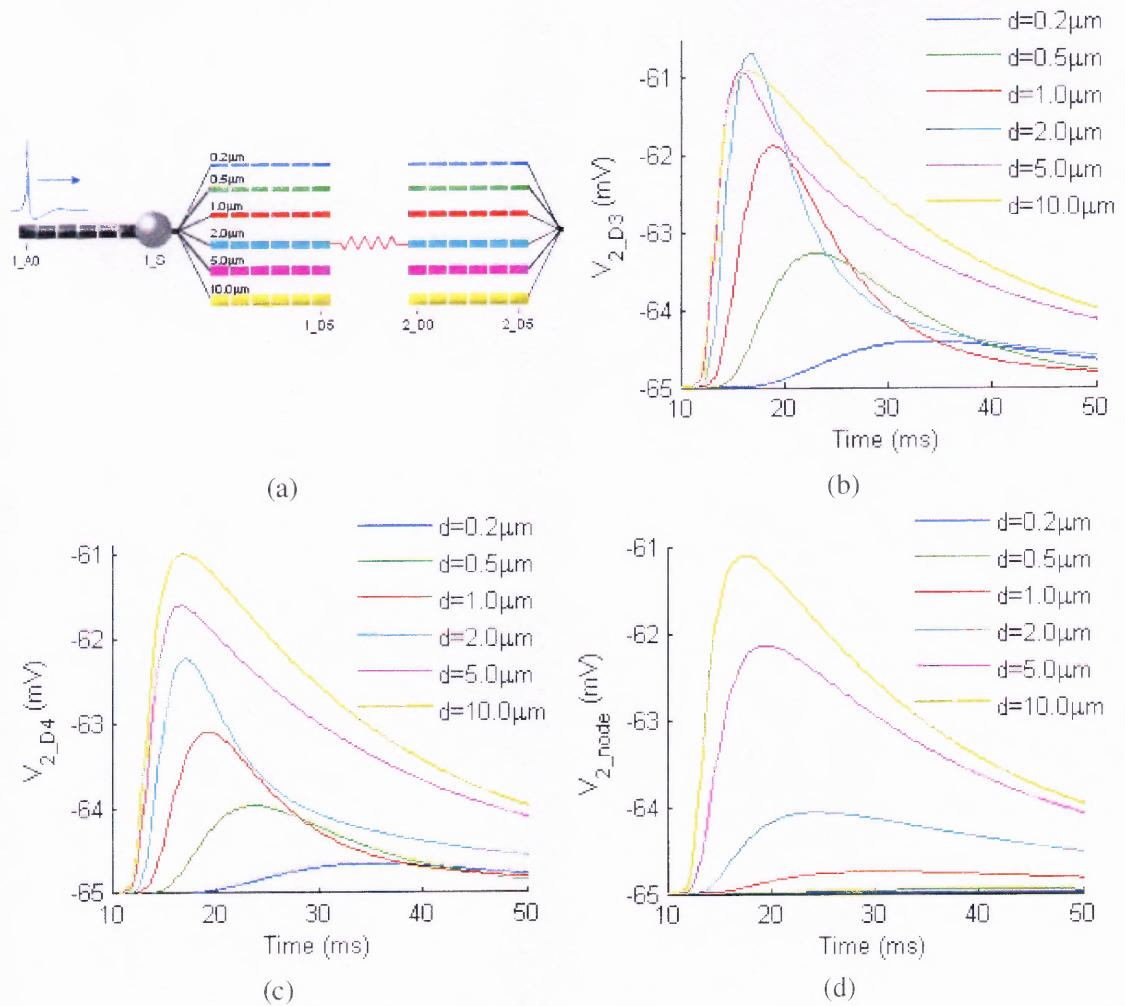
Figure 4.12 (a) Schematic of the modified setup of the multiple-dendrite model with the soma and the axon removed from the postsynaptic cell. (b-d) PSP at different locations of the dendrite and at the node of cell two, when a cell with several dendrites was electrically coupled to a dendrite of diameter d. The potential for the first compartments of the postsynaptic dendrite was similar to that shown in Figure 4.11a.

In order to examine if the branching of the dendrite into several other dendrites at the node eliminates the optimal diameter, the model was modified and the postsynaptic soma and axon were removed (Fig. 4.12a). Although the voltage in the first compartment of the postsynaptic dendrite was again maximal for $d = 2\mu$m, this optimal diameter disappeared from the fifth compartment on, where the potential was maximal for the largest diameter. As expected from the preceding results, there was a sharp decline of the potential for small diameters at the compartments close to the branching point and in the node itself (Fig. 4.12b-d).

(a)

(b)

(c)

(d)
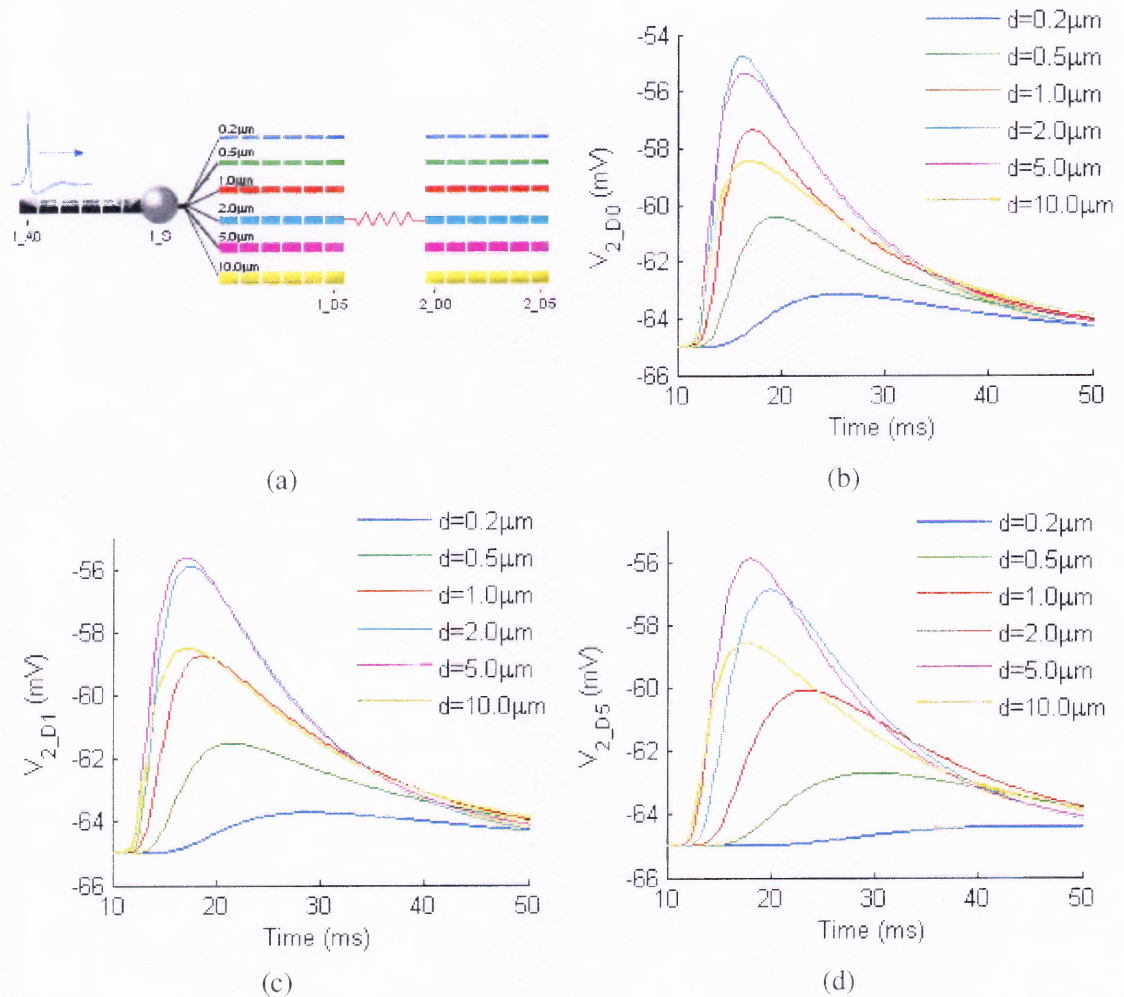
Figure 4.13 (a) Schematic of the modified setup of the multiple-dendrite model with only a single dendrite coupled to the presynaptic cell. (b-d) Potential at different locations of the postsynaptic dendrite when coupled to a presynaptic cell with several dendrites of diameter d.

In contrast, when the node was removed and only a single dendrite was coupled to the presynaptic cell, an optimal diameter of $d = 5\mu$m existed (Fig. 4.13). However, in the most distal compartment of the postsynaptic fiber the diameter for which the potential was optimized was again $d = 2\mu$m.

Next it was studied if an optimal diameter existed when the postsynaptic cell was represented by a ball-and-stick model (Fig. 4.14a). As in the case of a single dendrite, the potential measured in the postsynaptic soma was optimal for $d = 5\mu$m (Fig. 4.14b).

Using the same setup but replacing the postsynaptic cell by an equivalent dendrite-and-axon model as shown in Figure 4.15a, there was no optimal diameter (Fig. 4.15b).
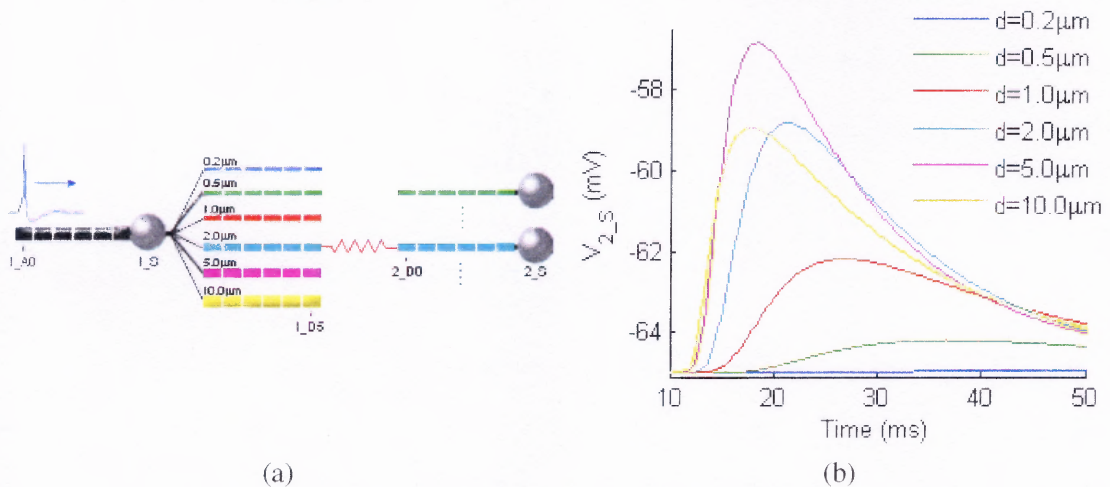
Figure 4.14 (a) Schematic of the modified setup of the multiple-dendrite model with the postsynaptic cell represented by a ball-and-stick model. (b) PSP in the soma for different diameters with the postsynaptic cell represented by a ball-and-stick model.

When changing the diameters of the pre- and postsynaptic dendrites to 4μm, 6μm, 8μm, 10μm, 12μm, and 14μm, the potential in the postsynaptic soma was maximal in amplitude for a diameter in the range 6μm to 10μm (Fig. 4.16). The amplitude of the potential was diminished for smaller or larger diameters.

In summary, the results of comparing the models with branching to the models without branching imply that the branching seems indeed to cause the absence of the optimal diameter.

4.3.4 Partially-Active-Dendrites Model

Studying the multiple-dendrite model revealed that signals transmitted by fibers of small diameter were shunted when they arrived at a branching point where other fibers emerged. Hence, an optimal diameter that existed at the other positions along the postsynaptic dendrite could not be observed in the proximal compartment of the fiber or in the soma. The idea of the model with partially active dendrites was to overcome voltage attenuation for the dendrite with the optimal diameter by amplifying the potential prior to its arrival at the node. It is now widely accepted that voltage-gated ion channels are expressed in parts of the dendrites (Saraga et al., 2003; Johnston et al., 2003; Cook and Johnston, 1999). In the

(a)   (b)
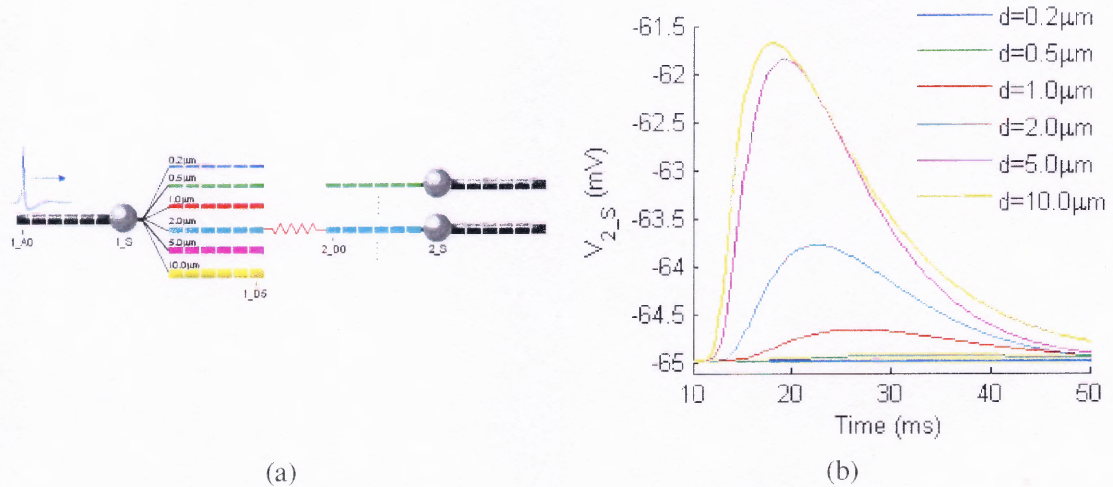
Figure 4.15 (a) Schematic of the the setup when the postsynaptic cell consisted of a dendrite, a soma, and an axon. (b) The PSP measured in the soma.
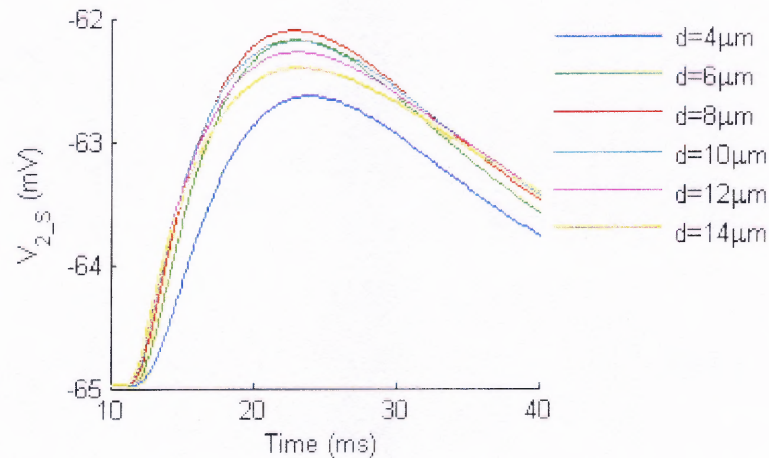

Figure 4.16 PSP in the soma for different diameters with the postsynaptic cell represented by a dendrite-and-axon model. The amplitude of the potential for the diameters in the range 6-10μm was almost the same. However, for smaller and larger diameters the PSP was smaller in amplitude.
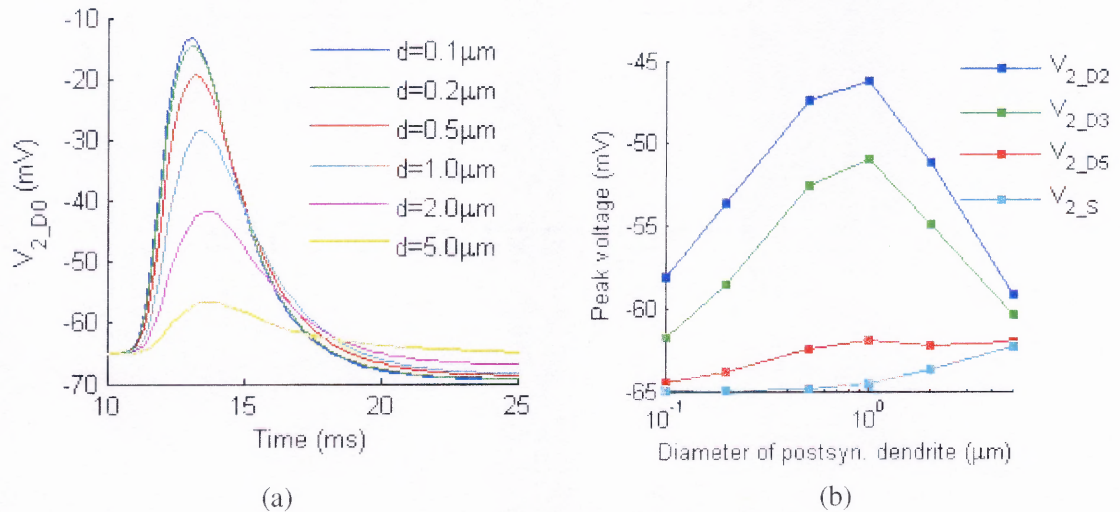
Figure 4.17 (a) Voltage versus time for the distal compartment of the postsynaptic dendrite for different diameters. The potential was a decreasing function of the diameter. (b) Peak voltage versus diameter for different locations on the postsynaptic neuron. There was no optimal diameter for the soma.

model at hand it was supposed that the active properties accumulate at the proximal half of the postsynaptic dendrite.

Using this model the optimal diameter was detected when the threshold was not changed. Because the presynaptic neuron was fixed, the peak potential at the distal segment of the presynaptic dendrite was almost the same, independent of the coupling to the postsynaptic cell. As a consequence of Equation (3.10) the potential at the first compartment of the postsynaptic dendrite was only dependent on its input resistance and was therefore a decreasing function of the diameter (Fig. 4.17a).

Except for the distal compartment, there existed an optimal diameter ($d = 1\mu$m) for all positions of the postsynaptic dendrite (Fig. 4.17b). At the soma the load of the other dendrites emerging from the node attenuated the signal and eliminated the optimal diameter.

Reducing the threshold by 5.2mV, an action potential in the fourth compartment of the postsynaptic dendrite was triggered for a diameter of 0.5μm (Fig. 4.18a). Reducing the threshold led again to a decrease of the optimal diameter. Owing to the branching, the signal was sharply attenuated when it arrived at the soma (Fig. 4.18b). Although an action potential was initiated for $d = 0.5\mu$m, the amplitude of the potential at the soma was lower
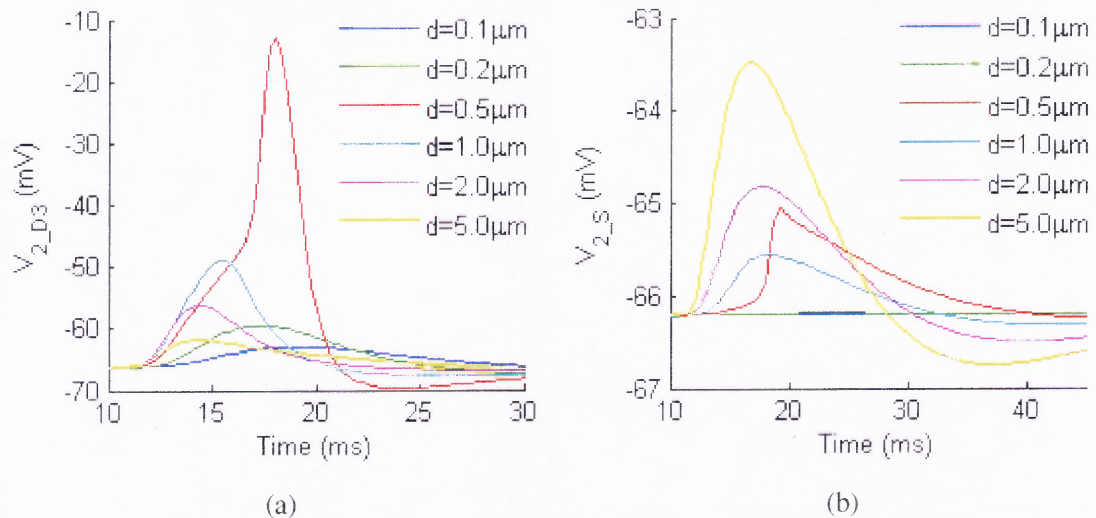
Figure 4.18 Voltage in the postsynaptic neuron when the threshold was reduced by 5.2mV. (a) Potential in the fourth compartment of the dendrite. An action potential was initiated for $d = 0.5\mu$m. (b) Voltage in the postsynaptic soma. The signal was shunted for dendrites of small diameter.

than the amplitude of the potential for $d = 2\mu$m or $d = 5\mu$m. The shunted action potential for $d = 0.5\mu$m had a distinct shape in comparison to the graded potentials that traveled passively toward the soma.

4.4   Models of Small Networks

In the last section it has been demonstrated that for ball-and-stick and dendrite-and-axon neurons, the initiation of an action potential is linked to the diameter of the connected fibers. An action potential is triggered only if the diameter of the postsynaptic dendrite has the optimal value. The impact of these results on networks formed by dendrite-and-axon neurons is addressed in the following sections. First, the investigated models are introduced in Sections 4.4.1 and 4.4.2. Next, the results of the simulations are presented in Section 4.5.

4.4.1   Ring Model with Asymmetric Gap Junctions

In a ring model, six or 10 neurons, respectively, were alternately coupled by asymmetric gap junctions, axon to axon, and dendrite to dendrite (Fig. 4.19a). The gap junctions permitted clockwise current flow between two adjacent neurons and prohibited flux in the
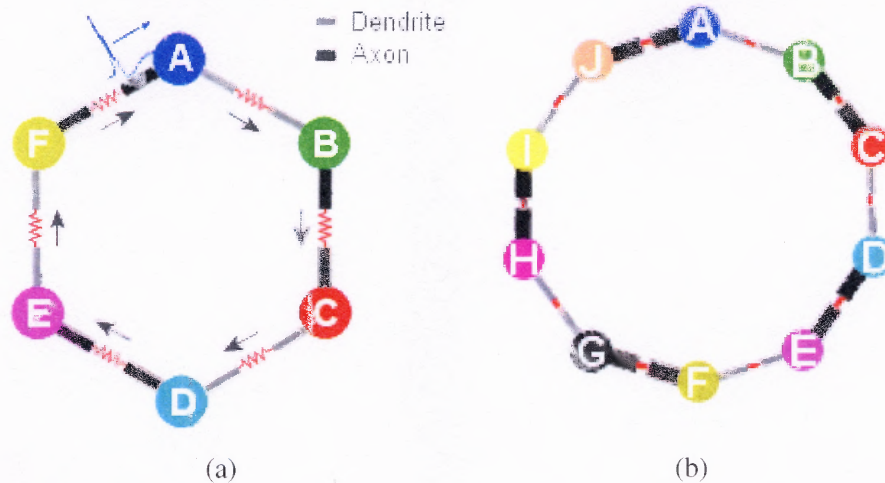
Figure 4.19 (a) Illustration of the ring model with six neurons coupled by asymmetric gap junctions. Current flux is permitted only in the direction indicated by the arrows. (b) Representation of the ring model with 10 neurons.

opposite direction. The neurons were resembled by the dendrite-and-axon model introduced in Section 4.2.3.

A current of 10nA was applied for 2ms into the distal compartment of the axon of neuron A in order to initiate an action potential.

4.4.2 Ring Model with Symmetric Gap Junctions

A ring of 10 neurons coupled by symmetric electrical synapses was built. The neurons were represented by dendrite-and-axon models (Fig. 4.19b). The length of the neurites was reduced by one-third to 400μm each, and they were compartmentalized into four segments of equal length.

A current of 3nA was applied for 2ms into the proximal compartment of the axon of neuron A for the purpose of initiating an action potential.

4.5   Results for Small Networks

4.5.1   Ring Model with Asymmetric Gap Junctions

In this model, the current was prohibited from flowing counterclockwise across the electrical synapse. Presuming a threshold reduced by 9.4mV, an action potential was propagated clockwise from neuron to neuron only if the dendrite's diameter was 5μm. As illustrated

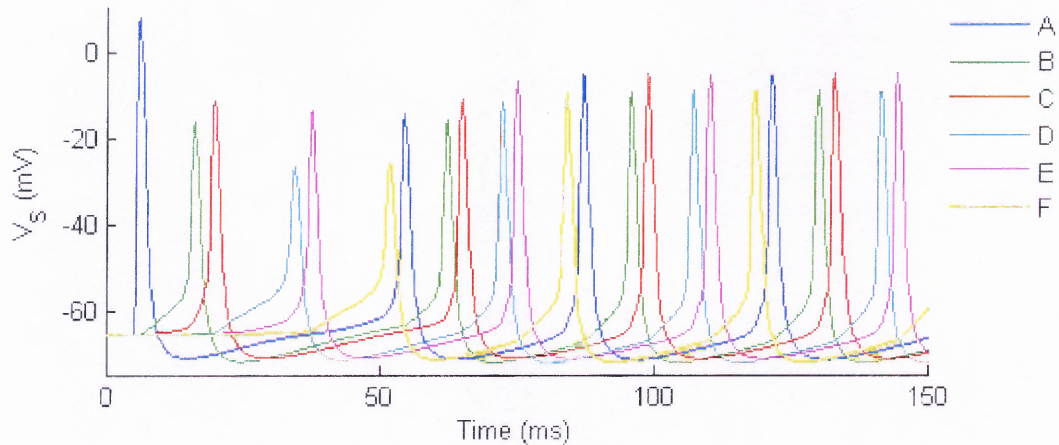**Figure 4.20** Ring model with six neurons. For cells with a dendrite of diameter 5μm, network activity could be established.

in Figure 4.20, it took about two cycles to establish periodical activity. This activity was self-sustained.

In order to demonstrate that this activity did not result from spontaneous firing of the individual neurons, but was indeed established by the propagation of action potentials from cell to cell, the ring was extended to a ring with 10 neurons. In Figure 4.21 the action potential propagation for this network is shown, and it can be seen that every neuron returned to its resting state before another action potential was triggered by the preceding cell.

The pattern of the activity was a result of the anatomy of the network. Signal conductance in the axons was faster than in the dendrites for the following reasons. First, the axon was twice as large in diameter as the dendrite, and therefore served as the better conductor. Second, the active properties of the axon counteracted the leak current and maintained the gradient along the fiber. Therefore, the delay between the action potentials in neurons coupled at the axons (e.g. B-C, D-E) was about half of the time lag between the action potentials of neurons connected by dendro-dendritic gap junctions.

If the diameter of the dendrites differed significantly from 5μm, the action potential was not propagated through the entire network. For diameters within two units of the optimal value, an action potential in cell B was triggered that consequently led to an
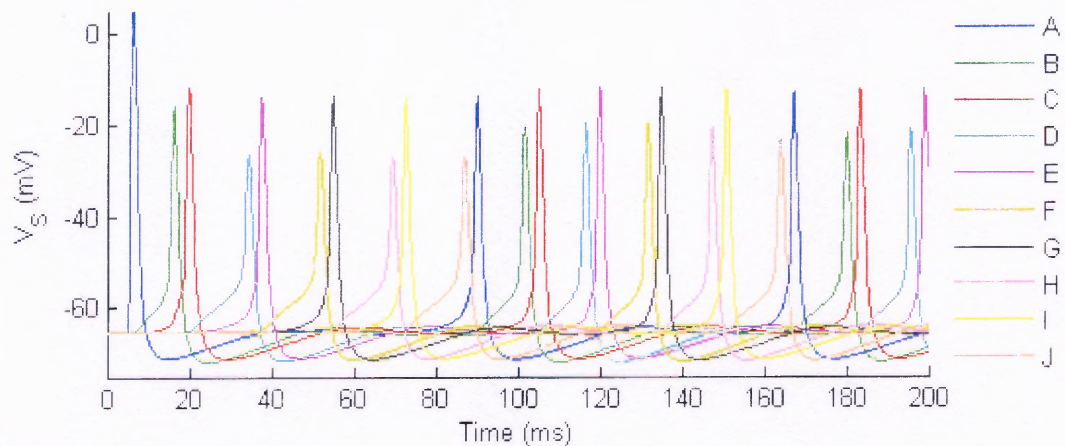
Figure 4.21 Action potential propagation in a ring model with 10 neurons; the dendrite's diameter was 5μm. The cells returned to their resting state before another action potential was initiated by the preceding neuron.

(a)   (b)

Figure 4.22 Potential versus time measured in the soma of the cells in a ring of six neurons. The threshold was reduced by 9.4mV. (a) For dendrites of a diameter within two units of the optimal value, the action potential was propagated into cells B and C (here: $d = 4\mu$m). (b) For diameters more than two units smaller or larger than the optimal value, the propagation of the action potential failed entirely (here for d=8μm).
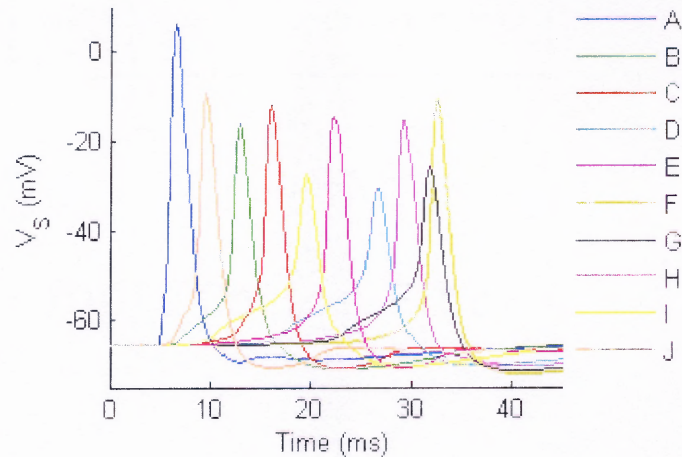
Figure 4.23 Action potential propagation and block by collision close to cell F in a ring model with 10 neurons coupled by symmetric gap junctions. The voltage was measured in the soma of the cells. The dendrite's diameter was 5μm, and the threshold was reduced by 9.5mV.

action potential in cell C because of axo-axonal coupling (Fig. 4.22a). Further increase or decrease however, resulted in the failure of the action potential propagation into cell B (Fig. 4.22b). In accordance with the observations made earlier, spontaneous spiking occurred for dendrites of a small diameter ($d \leq 0.5\mu$m).

4.5.2 Ring Model with Symmetric Gap Junctions

In this model the gap junctions were symmetric, as in the studies on coupling between two neurons discussed in Sections 4.2 and 4.3. The length of the neurites was decreased in order to increase the amplitude of the potential to a value significantly higher than the resting potential.

Presuming a threshold reduced by 9.5mV, an action potential initiated in the proximal compartment of the axon of cell A failed to propagate through the entire ring if the diameter of the dendrite was significantly different from 5μm. For neurons with dendrites of a diameter of 5μm, one action potential was propagated clockwise and another one was propagated counterclockwise until they collided near cell F. Since both adjacent cells were in their refractory period, the action potential was not conducted further (Fig. 4.23).
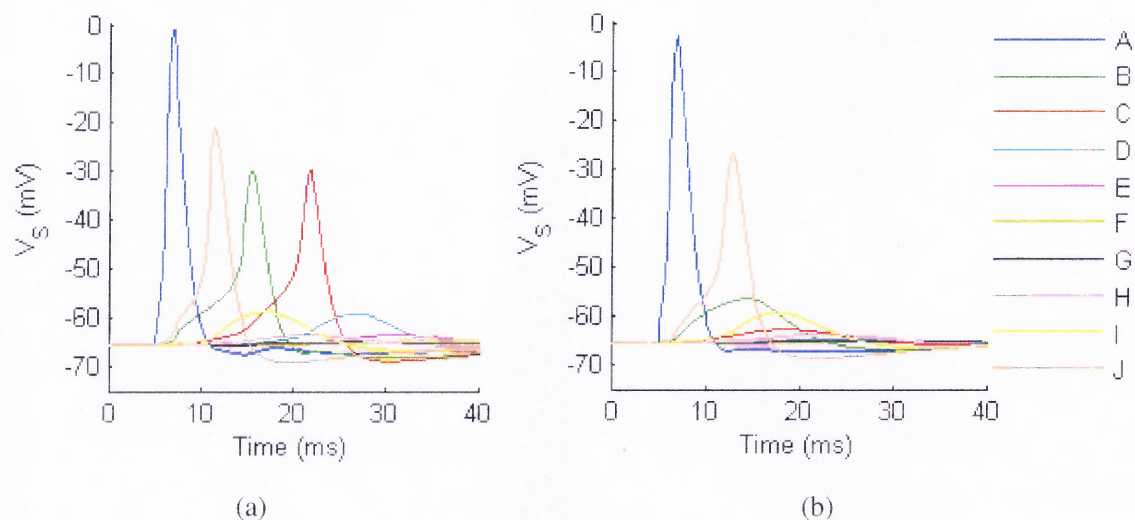
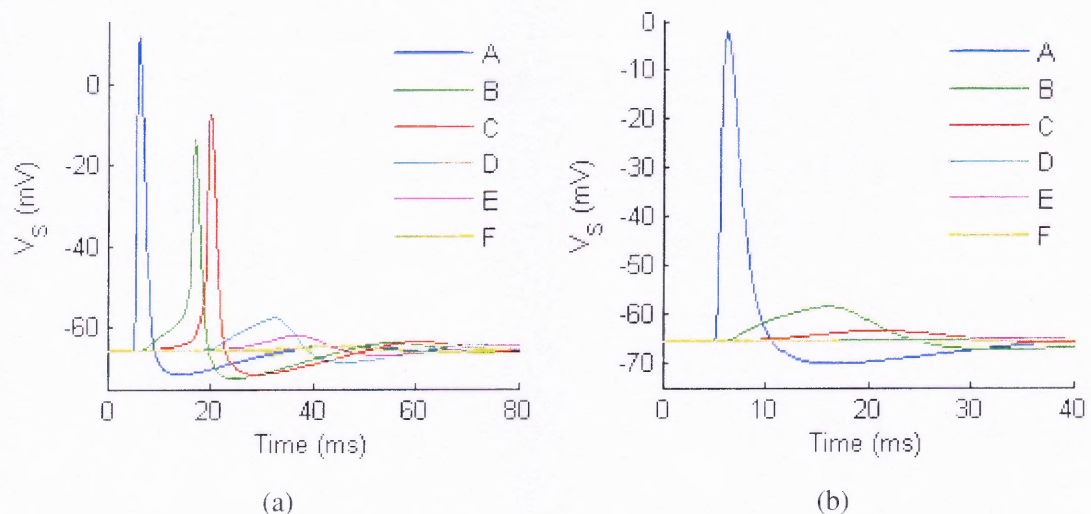**Figure 4.24** Potential versus time measured in the soma of the cells in the network. The threshold was reduced by 9.5mV. (a) For a diameter within three units of the optimal value, the action potential was not propagated further than two cells clockwise and one cell counterclockwise (here: $d = 8\mu$m). (b) Decreasing or increasing the diameter further, the action potential is only propagated into the axo-axonal coupled cell J (here: $d = 9\mu$m).

For diameters within three units of the optimal value, the action potential was propagated only to the cells adjacent to the point of current injection, and from cell B to cell C because of the axo-axonal coupling (Fig. 4.24a). For diameters smaller or larger, an action potential was only triggered in cell J since its axon was connected to the axon of cell A (Fig. 4.24b). For neurons with dendrites smaller than or equal to 0.5μm, spontaneous spiking activity was observed.

CHAPTER 5

CONCLUSION

In recent years, electrical coupling via gap junctions has been found to occur more frequently than previously conjectured. In the developing central nervous system, gap junctionally coupled neurons form large, functional clusters, which are refined during adolescence (Hormuzdi et al., 2004). To foster an understanding of the contribution of the neuron's intrinsic characteristics on the network function, theoretical and computational methods are necessary, because in most cases the direct experimental manipulation of the properties of the neuron is not feasible.

In this thesis, the impact of the fiber's diameter on the efficacy of action potential initiation and propagation has been studied theoretically using simulations. Pairs of electrically coupled neurons as well as small, circular networks were investigated. Each neuron was compartmentalized and the segments were equipped with passive properties or Hodgkin-Huxley sodium and potassium currents, respectively.

For pairs of neurons represented by the ball-and-stick or the dendrite-and-axon model, an action potential is initiated only for fibers of a specific, optimal diameter. In contrast, for multiple-dendrite cells no optimal diameter exists. Instead, the signal transmission improves as the diameter of the connected fibers increases. In the postsynaptic cell the abrupt increase in membrane area to be charged results in a sharp attenuation of the signal, which is comparable to a so called "conduction block" (Quan and Rudy, 1990).

The goal of this thesis was to examine whether network activity arises from an optimal diameter of the coupled fibers. A small ring structure with neurons alternately coupled either at the axons or dendrites was examined. It has been demonstrated that the propagation of action potentials through the entire network is only successful for a specific diameter of the dendrites. If the neurons are connected by an asymmetric gap junction, the circular network exhibits self-sustained activity once an action potential is initiated by an external stimulus. Since dendro-dendritic coupling is abundant in the mammalian brain, it

should be examined whether the same network behavior also occurs for networks coupled exclusively by dendro-dendritic gap junctions.

Extensive networks of electrically coupled interneurons form in different regions of the brain, e.g. in the neocortex and the retina, and are assumed to be critical for the generation of oscillations and synchronous activity (Amitai et al., 2002; Gibson, Beierlein, and Connors, 1999). For small networks the impact of the fiber's diameter on signal propagation has been demonstrated. However, the question if the activity in large networks arises only for fibers of the optimal diameter remains to be answered and will be the subject of future research in this area.

REFERENCES

Amitai, Y., Gibson, J. R., Beierlein, M., Patrick, S. L., Ho, A. M., Connors, B. W., and Golomb, D. (2002). The spatial dimensions of electrically coupled networks of interneurons in the neocortex. *J Neurosci* 22(10): 4142–4152.

Arroyo, E. J. and Scherer, S. S. (2000). On the molecular architecture of myelinated fibers. *Histochem Cell Biol* 113(1): 1–18.

Beierlein, M., Gibson, J. R., and Connors, B. W. (2000). A network of electrically coupled interneurons drives synchronized inhibition in neocortex. *Nat Neurosci* 3(9): 904–910.

Bennett, M. V. L. and Zukin, R. S. (2004). Electrical coupling and neuronal synchronization in the mammalian brain. *Neuron* 41(4): 495–511.

Bernstein, J. (1902). Untersuchungen zur Thermodynamik der bioelektrischen Ströme. *Pflügers Arch* 92: 521–562.

Cook, E. P. and Johnston, D. (1999). Voltage-dependent properties of dendrites that eliminate location-dependent variability of synaptic input. *J Neurophysiol* 81(2): 535–543.

Curtis, H. J. and Cole, K. S. (1942). Membrane resting and action potentials from the squid giant axon. *J. Cell. & Comp. Physiol.* 19: 135–144.

Dayan, P. and Abbott, L. F. (2001). *Theoretical Neuroscience: Computational and Mathematical Modeling of Neural Systems.* The MIT Press.

Fukuda, T. and Kosaka, T. (2003). Ultrastructural study of gap junctions between dendrites of parvalbumin-containing GABAergic neurons in various neocortical areas of the adult rat. *Neuroscience* 120(1): 5–20.

Gibson, J. R., Beierlein, M., and Connors, B. W. (1999). Two networks of electrically coupled inhibitory neurons in neocortex. *Nature* 402(6757): 75–79.

Hampson, E. C., Weiler, R., and Vaney, D. I. (1994). pH-gated dopaminergic modulation of horizontal cell gap junctions in mammalian retina. *Proc Biol Sci* 255(1342): 67–72.

Hodgkin, A. L. and Huxley, A. F. (1945). Resting and action potentials in single nerve fibres. *J Physiol* 104: 176–195.

Hodgkin, A. L. and Huxley, A. F. (1952). A quantitative description of membrane current and its application to conduction and excitation in nerve. *J Physiol* 117(4): 500–544.

Hormuzdi, S. G., Filippov, M. A., Mitropoulou, G., Monyer, H., and Bruzzone, R. (2004). Electrical synapses: a dynamic signaling system that shapes the activity of neuronal networks. *Biochim Biophys Acta* 1662(1-2): 113–137.

Johnston, D., Christie, B. R., Frick, A., Gray, R., Hoffman, D. A., Schexnayder, L. K., Watanabe, S., and Yuan, L. (2003). Active dendrites, potassium channels and synaptic plasticity. *Philos Trans R Soc Lond B Biol Sci* 358(1432): 667–674.

Kandel, E. R., Schwartz, J. H., and Jessell, T. M. (2000). *Principles of Neural Science.* McGraw-Hill Medical.

Kandler, K. and Katz, L. C. (1998). Coordination of neuronal activity in developing visual cortex by gap junction-mediated biochemical communication. *J Neurosci* 18(4): 1419–1427.

Keener, J. and Sneyd, J. (2001). *Mathematical Physiology.* Springer.

Koch, C. (1999). *Biophysics of Computation: Information Processing in Single Neurons (Computational Neuroscience Series).* Oxford University Press, USA, first edition.

Koch, C. and Segev, I. (1998). *Methods in Neuronal Modeling: From Ions to Networks (Computational Neuroscience).* The MIT Press, second edition.

Landisman, C. E. and Connors, B. W. (2005). Long-term modulation of electrical synapses in the mammalian thalamus. *Science* 310(5755): 1809–1813.

LeBeau, F. E. N., Traub, R. D., Monyer, H., Whittington, M. A., and Buhl, E. H. (2003). The role of electrical signaling via gap junctions in the generation of fast network oscillations. *Brain Res Bull* 62(1): 3–13.

Mamiya, A., Manor, Y., and Nadim, F. (2003). Short-term dynamics of a mixed chemical and electrical synapse in a rhythmic network. *J Neurosci* 23(29): 9557–9564.

Marder, E. (1998). Electrical synapses: beyond speed and synchrony to computation. *Curr Biol* 8(22): 795–797.

Nadim, F. and Golowasch, J. (2006). Signal transmission between gap-junctionally coupled passive cables is most effective at an optimal diameter. *J Neurophysiol* 95(6): 3831–3843.

Nicholls, J. G., Martin, A. R., Wallace, B. G., and Fuchs, P. A. (2001). *From Neuron to Brain: A Cellular and Molecular Approach to the Function of the Nervous System.* Sinauer Associates, fourth edition.

No author (2005). Wikipedia: Action potential. Retrieved February 18, 2006, from `http://en.wikipedia.org/wiki/Action_potential`.

Quan, W. and Rudy, Y. (1990). Unidirectional block and reentry of cardiac excitation: a model study. *Circ Res* 66(2): 367–382.

Saraga, F., Wu, C. P., Zhang, L., and Skinner, F. K. (2003). Active dendrites and spike propagation in multi-compartment models of oriens-lacunosum/moleculare hippocampal interneurons. *J Physiol* 552(Pt 3): 673–689.

Sharp, A. A., Abbott, L. F., and Marder, E. (1992). Artificial electrical synapses in oscillatory networks. *J Neurophysiol* 67(6): 1691–1694.

Simon, A. M. and Goodenough, D. A. (1998). Diverse functions of vertebrate gap junctions. *Trends Cell Biol* 8(12): 477–483.

Traub, R. D., Pais, I., Bibbig, A., LeBeau, F. E. N., Buhl, E. H., Hormuzdi, S. G., Monyer, H., and Whittington, M. A. (2003). Contrasting roles of axonal (pyramidal cell) and dendritic (interneuron) electrical coupling in the generation of neuronal network oscillations. *Proc Natl Acad Sci U S A* 100(3): 1370–1374.

Traub, R. D., Whittington, M. A., Buhl, E. H., LeBeau, F. E. N., Bibbig, A., Boyd, S., Cross, H., and Baldeweg, T. (2001). A possible role for gap junctions in generation of very fast EEG oscillations preceding the onset of, and perhaps initiating, seizures. *Epilepsia* 42: 153–170.

Young, J. L. (no date). Nervous system: Nerve tissue. Retrieved February 18, 2006, from `http://training.seer.cancer.gov/module_anatomy/unit5_2_nerve_tissue.html`.

Zhang, L. I. and Poo, M. M. (2001). Electrical activity and development of neural circuits. *Nat Neurosci* 4 Suppl: 1207–1214.

Zoidl, G. and Dermietzel, R. (2002). On the search for the electrical synapse: a glimpse at the future. *Cell Tissue Res* 310(2): 137–142.